NASA/TM-20250005172

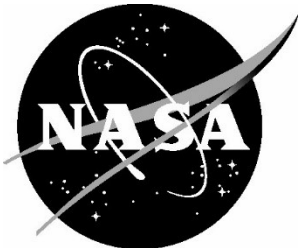

Vibratory Plate Compaction of BP-1 & LHS-1 Utilizing the Planetary Automated Compaction Tool (PACT)

E. A. Bell[1], B. W. Kemmerer[2], N. J. Gelino[3], L. Sibille[4], G. M. Holmgren[5], P. F. Flowers[6], V. Rao-Aourpally[7]

[1]Swamp Works, NE-L6, Laboratories, Development, and Testing Division, Kennedy Space Center (KSC), National Aeronautics & Space Administration (NASA), Mailstop NE-L6, KSC, FL. 32899, evan.a.bell@nasa.gov

[2]Swamp Works, UB-E, Exploration & Research Technologies, KSC, NASA, Mailstop UB-E, KSC, FL. 32899, beverly.kemmerer@nasa.gov,

[3]Swamp Works, UB-E, Exploration & Research Technologies, KSC, NASA, Mailstop UB-E, KSC, FL. 32899, nathan.j.gelino@nasa.gov,

[4]Swamp Works, Astrion, Kennedy Space Center, NASA, Mailstop LASSO-13, KSC, FL. 32899, laurent.sibille-1@nasa.gov,

[5]Swamp Works, NE-L6, Laboratories, Development, and Testing Division, KSC, NASA, Mailstop NE-L6, KSC, FL. 32899, gary.holmgren@nasa.gov

[6]Redwire, 8226 Phillips Hwy, Suite 101, Jacksonville, FL, 322056, patrick.flowers@redwirespace.com,

[7]Redwire, 8226 Phillips Hwy, Suite 101, Jacksonville, FL, 322056, vineel.rao-aourpally@redwirespace.com.

National Aeronautics and
Space Administration

Kennedy Space Center
Florida

May 2025

Table of Contents

1. Abstract

The Multifunctional End Effector for Regolith Construction, Acquisition, and Transfer (MEERCAT) is a robotic arm end effector developed by the Swamp Works Granular Mechanics and Regolith Operations (GMRO) lab [1]. This system has several capabilities including excavation, trenching, regolith size screening, compaction, and geotechnical property measurement.

The NASA Tipping Point Project, Mason, led by Redwire Space, in partnership with the Swamp Works GMRO lab, has continued development and refinement of the PACT system's compaction capabilities, specifically, under the new moniker Planetary Automated Compaction Tool (PACT). A test campaign in ambient laboratory conditions was conducted using Black Point-1 (BP-1) and Lunar Highlands-1 (LHS-1) simulants in the GMRO's Big Bin test facility utilizing the Excavation Test Stand (ETS) 2-axis gantry. Along with this work a correlation curve was developed to estimate bulk surface compaction based on surface pocket penetrometer readings of penetration force into simulant.

The tests revealed the PACT system to be capable of achieving 80% relative density (%RD) in BP-1 and LHS-1 using a dual-mass excentric mass motor. Testing showed that the Spot compaction method was more capable of compaction at depth (below 51 mm) than the Raster method. Several other conclusions were made including that higher static compaction pressure improved compaction at depth, and that longer surface contact times provided diminishing returns on compaction performance. A correlation between the ambient testing in LHS-1 performed as part of this test campaign and previous work performed in-vacuum conditions using LHS-1 is also shown over a test sample set.

2. Introduction

Kennedy Space Center's Granular Mechanics and Regolith Operations Laboratory (a.k.a., Swamp Works) was contracted to collaborate with Redwire Space on the Mason Project which was awarded via a NASA Tipping Point. The Mason project objective is to develop systems capable of grading, compacting, and microwave sintering regolith for lunar infrastructure applications such as roads, launch/landing pads, and dust mitigation. Swamp Works was contracted to develop the compaction system for the project. The compaction system is based on previous work on the Multifunctional End Effector for Regolith Construction, Acquisition, and Transport system which has compaction functionality along with other capabilities including scooping, leveling and size screening regolith (Figure 1). Through testing on the Mason project in 2024 the team was able to further develop the plate compaction capabilities under the moniker Planetary Automated Compaction Tool (PACT).

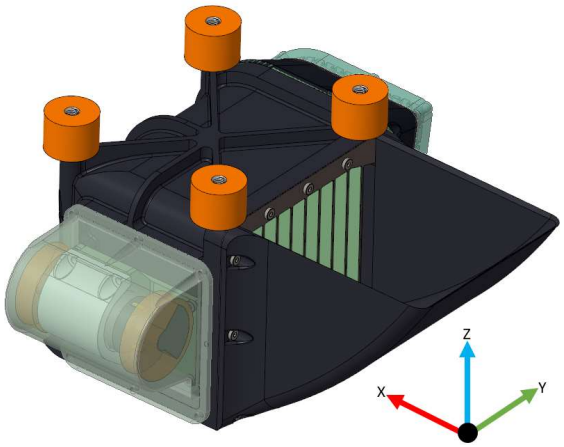

Figure 1. PACT & dual-mass motor in Y-Z force orientation.

3. Hardware Under Test – PACT

a. PACT Description

Figure 2 shows the hardware under test (the large scratches on the compaction surface are due to impact wear testing on 15 cm rock prior to compaction testing and are superficial to PACT testing). The compaction plate surface of PACT is a flat type III hard coat anodized 7075-T651 rectangular region measuring 90 mm in the X-axis and 120 mm in the Y-axis equaling 10,800 mm^2. For testing purposes, it is assumed the corner radii and excavation blade surfaces have minimal impact on compaction forces and were excluded in compaction pressure calculations. Orange high-temp silicone vibration dampeners (Techproducts 50860-5) are used to mate mobility systems using M6 fasteners. The grey dust cover houses the dual-mass vibratory actuator. A separate, black dust covering is used while utilizing the single-mass vibratory motor. These motors are described further in the following sub-section. The system mass is approximately 1200 grams with the dual-mass motor configuration.

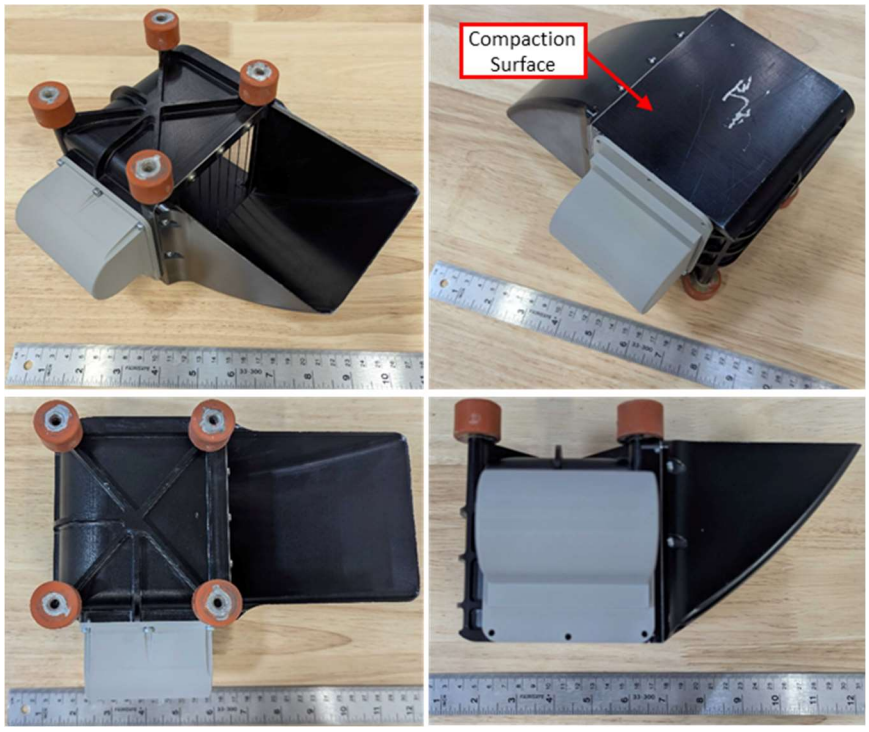

Figure 2. PACT Hardware.

b. Motor Configurations

PACT was tested in two vibratory motor configurations. The first configuration used a dual-mass vibe motor (Figure 3) installed so vibratory force was applied along the Z-Y plane, thus creating Z-axis up/down motion. This configuration was used for all BP-1 regolith Spot and Raster testing. This motor was a NFP model NFP-DH385-FS.

A second vibratory motor configuration using a single-mass motor oriented with vibratory force applied in the X-Y plane was used during LHS-1 testing to replicate the configuration during previous work performed with PACT in-vacuum. This motor was a non-branded motor rated to 4500 RPM at 12 V. An additional compaction test was performed in LHS-1 with the dual-mass Z-Y motor configuration. This was done to provide a comparison point between the dual-mass Z-Y motor and the single-mass X-Y motor and their effects on compaction in a common regolith simulant.

These two configurations are shown in Figure 4 with the direction of vibratory force represented as red dual-direction arrows.

Figure 3. Dual-mass Z-Y motor (left) and single-mass X-Y motor (right).

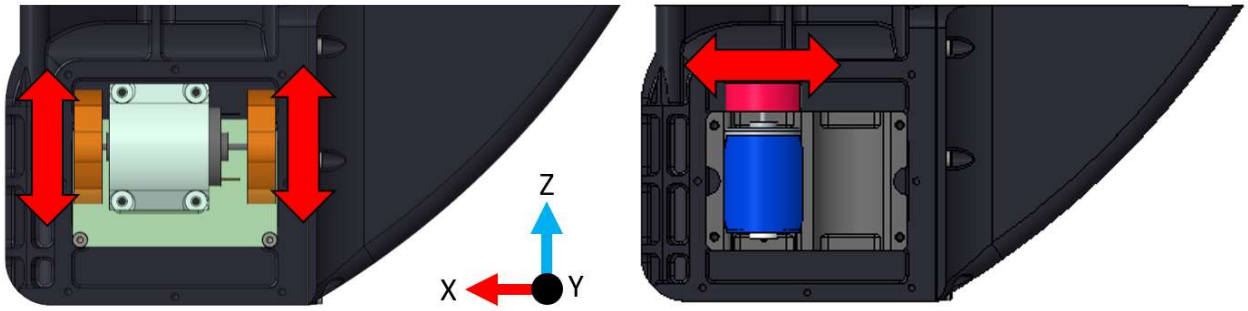

Figure 4. Dual-mass Z-Y motor config (left) and single-mas X-Y motor config (right).

4. Test Parameters

a. Desired Goal Relative Density

A goal of 80%RD for compacted surfaces was set. This relative density level is adequate for efficient sintering of regolith and is a good, reasonably achievable starting condition for other compaction applications. Parameter sets that did not regularly achieve 80%RD were considered ineffective at compaction. For BP-1 and LHS-1 a relative density of 80%RD corresponds to approximately 1.70 g/cm^3. The derivation of this is outlined in *Appendix B: Relative Density Calculations*.

b. Test Parameters

Eight test parameters were explored during the ambient compaction testing:

- Compaction method (referred to as "spot" and "raster" within this report)
- Vibratory frequency
- Static pressure (spot compaction motion only)
- Surface contact time
- Simulant
- Slope
- Initial bulk regolith density
- Pass depth (raster compaction motion only).

Table 1 shows the various test parameters.

Table 1. Compactor test parameters.

Test Parameter	Tested Values
Compaction Motion	Spot, Raster
Static Compaction Pressure (Spot Compaction Only)	7, 70 kPa
Pass Depth (Raster Compaction Only)	1 mm, 5 mm
Vibratory Frequency	0, 45, 71 Hz (Dual-Mass Motor) 158 Hz (Single-Mass Motor)
Surface Contact Time	5, 8, 10, 30, 180 seconds (spot)

	3.6, 6, 10 seconds (raster)
Simulant	BP-1, LHS-1
Initial Bulk Regolith Density (In percentage relative density)	59%RD (+/-3%RD)
Slope	0°

Compaction Motion

The compaction motion parameter refers to two potential modes of operation, spot compaction and raster compaction as seen in Figure 5.

Spot compaction applies a specified pressure to a location on the surface along with vibratory load. The system is allowed to sink freely into the granular material to maintain constant pressure. After a set amount of time the system is lifted and translated horizontally to a second location (with some overlap) and pressure is applied again. This sequence is repeated until the specified area is compacted.

Raster compaction positions the system into the regolith at a specified depth and then travels horizontally at that depth until the desired area has been compacted. During travel, vibratory load is applied, and a surcharge of regolith is pushed along with the system. No constant downward force is applied. The velocity of travel controls the total surface contact time which correlates to the total time a given regolith location is in contact with PACT's plate compaction surface. For example, the plate compaction surface on PACT is 90 mm along it's X-axis, when traveling at 9 mm/s the contact time is 10 seconds.

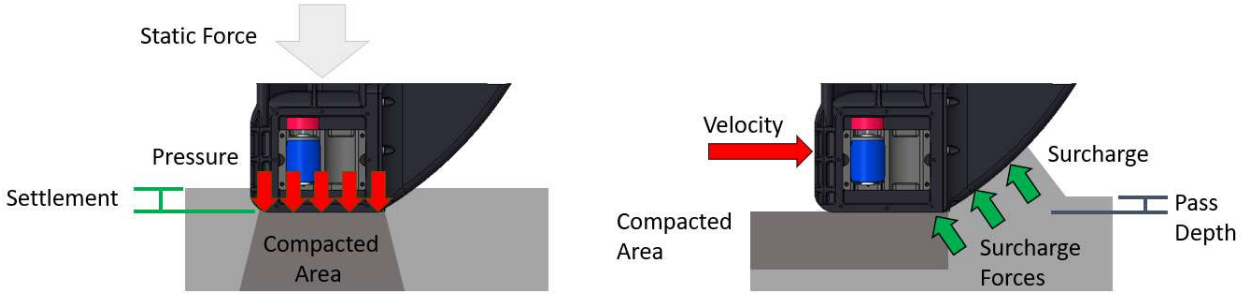

Figure 5. Spot compaction (left) and raster compaction (right).

Static Compaction Pressure (Spot Compaction)

For spot compaction tests, static compaction pressure was achieved using known mass weights (including the intrinsic weight of the PACT system). The calculated weights needed for a given pressure were based on the 120 mm x 90 mm surface area of the compaction plate on PACT. For 7 kPa tests an equivalent to 75 N (17 lbf) of weight was used. For 70 kPa an equivalent to 750 N (170 lbf) of weight was used. Static pressure was not used in raster testing.

Note that 70 kPa tests represent a high static compaction pressure case and are included to show an extreme case higher than what is reasonably expected at a robotic scale for the given plate compactor size. The 750 N of weight added to the test unit caused unexpected deformation of the assembly that may have affected loadcell readings but did not appear to cause binding of the linear rail system which was rated by the manufacturer for the applied loading. It was assumed that the

full 70 kPa of static compaction pressure was applied to the regolith simulant in those cases. In raster compaction, the static compaction pressure is 0 kPa.

Pass Depth (Raster Compaction)

The pass depth parameter was explored in raster compaction tests. For BP-1 testing, a path depth of 5 mm was used for most tests. A single test was performed at a pass depth of 1 mm.

In the case of LHS-1 testing in the ambient bed, the chosen approach aimed at replicating the compactor plate contact pressure on the regolith selected for previous in-vacuum tests of the same plate using LHS-1 to allow direct comparisons from ambient to vacuum test results. The pass depth was set by lowering the compactor into the surface of the regolith until 70 kPa of pressure was applied to the compactor plate and then Raster compaction was performed as usual. This resulted in pass depths of 6.2, 8.3, and 16 mm in the three LHS-1 Raster compaction tests. Pass depth is not a parameter for the spot compaction method.

Vibration Frequency

The vibration frequency was set by providing a vibration motor with 24 V for 71 Hz and 12 V for 45 Hz. All BP-1 testing was done using a dual-mass motor. However, to align the LHS-1 with previous in-vacuum testing, a higher frequency, single-mass motor was used and powered with 24 V for a 158 Hz vibration frequency. Table 2 specifies the motor and the measured frequency. The frequency measured is based on the revolutions per second of the excentric mass on the motors using a Neiko 20713A handheld laser tachometer. Tests without vibratory actuation (a.k.a. 0 Hz) were added during testing to isolate the effects of vibration from that of static compaction pressure.

Table 2. Motor frequency readings via tachometer.

Motor Configuration	Tachometer Reading
Dual-Mass Motor (24 V) *NFP model NFP-DH385-FS*	71 Hz
Dual-Mass Motor (12 V) *NFP model NFP-DH385-FS*	45 Hz
Single-Mass Motor (24 V) *No Model Information*	158 Hz

Surface Contact Time

Surface contact time is the total time the compactor place is in contact with a given area of regolith. Originally, for spot compaction the system was to perform contact times of 10, 30, and 180 seconds. During data review, it was observed that some of the 10 seconds tests only showed contact for 5 and 8 seconds. The 180 seconds tests performed was reduced during testing as it was observed that compaction settlement no longer occurred after several seconds into compaction and compaction level of the regolith did not vary significantly between 30 and 180 seconds of contact time. This is highlighted through the results further in the report.

For raster compaction, the system is continually moving. Contact time equates to the time a given area of regolith is under any portion of the compactor plate. Given a 90 mm long compaction surface in the X-axis travel direction for raster compaction, contact times can be achieved with a

calculated, continuous travel speed. Testing with 30- and 180-seconds contact times would have drastically extended individual testing run durations well beyond what may be reasonable for a real lunar mission. For example, a 180 second contact time equates to a 0.5 mm/s velocity of the compactor. At that velocity a 1500 mm compaction length would take 50 minutes per pass and a Raster compaction test required 3 individual passes at the prescribed depth. The contact times for Raster compaction tests were changed to include testing at 3.6 seconds (25 mm/s velocity) and 6 seconds (15 mm/s velocity).

Simulant

Lunar Highlands Type 1 Glass (ICN-LHT-1G) simulant was initially down selected for use during PACT testing due to its lunar representative geotechnical characteristics. ICN-LHT-1G was not available in the necessary quantity within the project schedule constraints. Black Point 1 (BP-1) was instead chosen to be used for the majority of testing due to its representative geotechnical characteristics and availability at the GMRO laboratory. Lunar Highlands Simulant 1 (LHS-1) was also used for selected tests to compare previous compaction testing in-vacuum with compaction in ambient using similar test setups.

Initial Density

The initial state of the regolith after preparation was measured using a pocket penetrometer, cone penetrometer, and in some cases a core sampler (detailed in section 5.g). Using the pocket penetrometer data, the regolith simulant surface density was estimated. The conversion from the pocket penetrometer's dial reading to regolith simulant density and how it was derived is outlined in *Appendix A: Estimation of Bulk Density with Pocket Penetrometer Tests (PPT)* and *Appendix B: Relative Density Calculations*. The average pocket penetrometer reading was 7.3 kPa of pressure for the prepared surfaces during testing. This corresponds to an absolute density of about 1.55 g/cm^3 or 57% relative density. It was not practical to create initial densities of 48% or less as specified by the requirements and test parameters, but it is assumed that the compaction processes are not affected by lower initial densities.

The cone penetrometer readings were performed at approximately 51, 76, 102, 127, 152, 178, and 203 mm depths (2, 3, 4, 5, 6, 7, and 8 inches). While it is possible to develop a BP-1, or other simulant soil, correlation between cone penetrometer force reading and density as a specific depth, this was not completed as part of this work. These readings represent a relative difference in soil density between compaction tests given a similar low-density starting condition.

Slope

While the slope of the regolith relative to the compactor tool was considered for addition to the testing matrix, testing was limited to 0° (horizontal) only. The team concluded that for an arm mounted system or one attached to a mobility platform such as a rover, the compactor would likely be aligned with the slope of the regolith to be compacted. While the relative angle of the gravity vector compared to the regolith surface may influence final compaction, its effects are expected to be somewhat limited and outside the scope of early lunar construction demonstrations.

5. Test Setup and Operations

a. BP-1 Bin "Big Bin"

BP-1 compaction testing occurred within the GMRO lab's Big Bin. The Big Bin is approximately 7.7 x 7.3 m with BP-1 at 1 m deep. Within the Big Bin is the Excavator Test Stand (ETS).

Figure 6. Big Bin BP-1 test area with ETS (left).

b. Excavation Test Stand

The ETS was used inside of the Big Bin to execute testing (Figure 7). ETS was developed under previous work to characterize various parameters for bucket drum excavators and was retrofitted for this PACT testing. [2] The ETS is a two degree of freedom gantry system with travel of approximately 5 m along the horizontal axis and approximately 1 m travel along its vertical axis. The ETS is controlled using a LabVIEW user interface. The ETS force in the horizontal axis is limited to 300 N. While the ETS was designed with high travel velocities and accelerations for future use as a gravity-offload fixture, for the compaction testing, velocities were limited to 400 mm/s or less in X and 25 mm/s in Z. For Raster compaction testing, the X-axis travel rate was set to a fixed value to achieve the desired contact times. For a surface contact time of 30, 10, 6, and 3.6 seconds an X axis speed of 3, 9, 15, and 25 mm/s were used respectively.

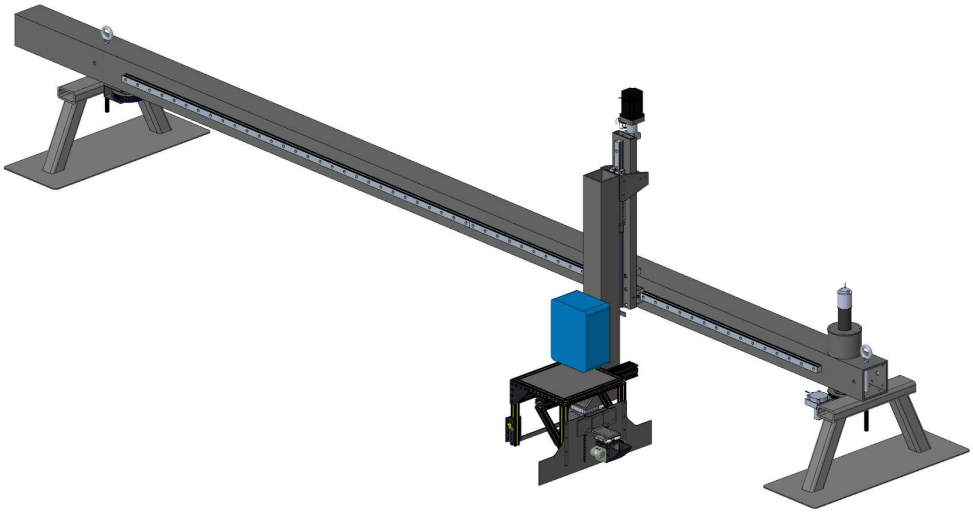

Figure 7. PACT on the ETS.

c. LHS-1 Bin

For LHS-1 testing, the container and surface preparation process replicated methods used in previous compaction experiments with PACT and LHS-1 in vacuum (Figure 8). The container was a 35.5 cm deep aluminum trapezoidal shape with an upper major area of 78.7 x 45.7 cm and a lower minor area of 43.1 x 38.1 cm resulting in a volume of 0.09 m^3. The LHS-1 container had to be placed under the ETS within the lab's the BP-1 Big Bin. A tarp was used to present cross contamination of simulants.

Figure 8. Trapezoidal LHS-1 bin within the BP-1 Big Bin after a spot compaction test.

d. PACT Assembly Installation

The PACT assembly was installed on the vertical axis of the ETS as seen in Figure 9. In the assembly, PACT was attached to two 500 N ATO tri-axial load cells (ATO-LCMA-DYDW-005). The load readings of the two load cells are summed for a total read range of 0 to 1000 N (which equates to 0 to 92.6 kPa surface pressure for the PACT system). The axis orientation of the load cell readings is shown in Figure 9. The load cells were attached to a bracket that could

accommodate weights to achieve specified compaction pressures. The bracket was also connected to two vertical linear rails that would allow PACT and the weights to "float" vertically relative to the ETS when PACT's compaction surface was placed on the regolith surface. Settlement into the regolith was visually read using 1 mm increment witness marks to the side of the linear rail. This configuration was used for spot compaction tests. During raster compaction tests the linear rails were locked at the bottom of the travel so that a specified fixed pass depth into the regolith could be achieved through commanding the vertical axis of the ETS. This hardware was connected to a surface-leveling blade that was used to smooth out the prepared regolith surface and ensure that PACT's compaction force was normal to the surface. The blade and PACT assembly were attached to the vertical axis of the ETS.

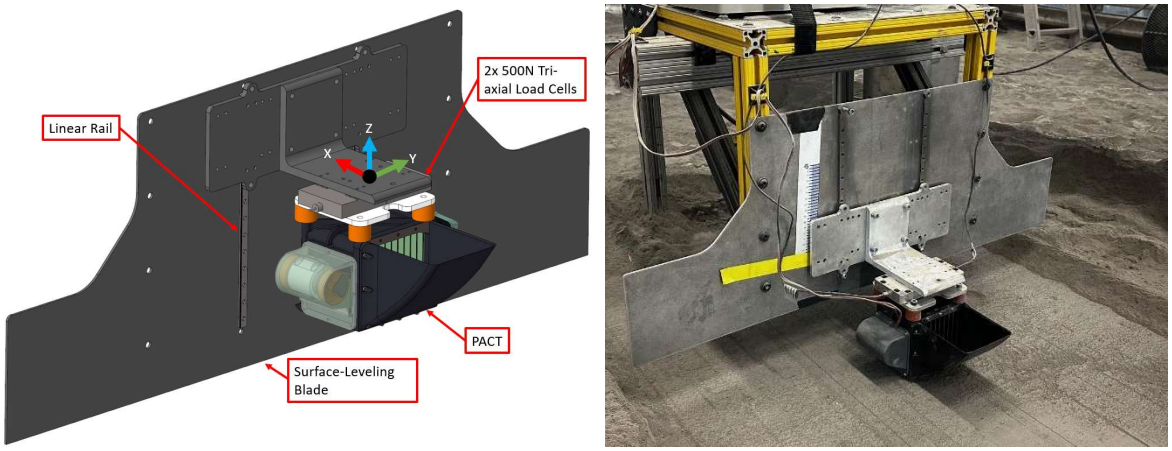

Figure 9. PACT on Surface-Leveling Tool (which is attached to the ETS).

e. Test Area Simulant Preparation

Testing was performed in both BP-1 and LHS-1. For each regolith simulant a different test area preparation was performed. Preparing the regolith simulant was done with care to attempt to create consistent test conditions. It is challenging and time consuming to prepare the test area with precision.

For BP-1 compaction tests, the area was prepared by shoveling a 0.3 m deep pit with horizontal dimensions of 0.6 x 0.6 m for Spot compaction and 0.6 x 1.8 m for Raster compaction. A mesh screen with 1 cm holes was placed over the pit. The excavated material was then shoveled onto the mesh which allowed the pit to be filled with relatively consistent low density regolith simulant. The mesh also sieved out any particles above 1 cm diameter. The pit was filled to as close to a uniform height as possible using this method. Figure 10 shows test operators excavating a pit and filling back in a pit via the screen mesh.

Figure 10. A pit is dug, and a previously excavated pit is covered by the 1 cm mesh screen and refilled with low density bulk regolith.

After filling the pit, the mesh was removed. The surface was gently raked to further level the surface. This action tended to slightly increase the density on the surface. Following the manual preparation, the ETS grader was commanded to pass back and forth across the test surface in 0.5 mm depth increments to provide the final surface with the vertical axis of the ETS normal to the surface plane. ETS grading resulted in an additional slight increase in density of the surface regolith. This preparation method resulted in a reasonably consistent regolith simulant test bed. The final surface finish can be seen in Figure 11.

Figure 11. BP-1 surface after preparation and leveling.

For LHS-1 bin preparation, a pit was excavated in the BP-1 that was larger than the LHS-1 container. To prevent cross-contamination of the LHS-1 and BP-1 simulants, a tarp was laid down on in the pit on the BP-1 and the LHS-1 container was placed on top. The top of the container was approximately level to the surrounding BP-1 surface. The LHS-1 was carefully shoveled from buckets into the container in thin layers to preserve the low-density condition. After filling the

container, the surface was gently leveled with a rake in a crosshatch pattern resulting in a somewhat irregular surface, shown in Figure 12. The processes of removing the LHS-1 from the trapezoidal bin and replacing it was completed for each test in ambient. Test operations for LHS-1 differed from BP-1 and are described in section 5.f.

Figure 12. LHS-1 bin final raked surface before a compaction test begins.

f. Previous Vacuum Compaction Test Set-Up and Operations

Previous compaction testing was completed in the Atmospherically Sealed Simulator for In-situ System Testing (ASSIST) Dirty Thermal Vacuum (DTVAC) chamber with the same container, LHS-1 simulant type, and version of PACT. The vacuum testing used the Advanced Regolith Ground Operations (ARGO) gantry to provide motion [3]. A single axis load cell (Futec LCM300) was placed between PACT and ARGO to record and verify compaction pressure.

The simulant was prepared and manually leveled in ambient conditions as described above. The chamber was then pumped down. A final leveling pass was completed with PACT under vacuum prior to compaction testing. Vacuum levels of $8x10^{-3}$ Torr or lower were achieved during testing.

The compaction test operations using LHS-1 differed from those of BP-1. For both ambient and vacuum LHS-1 tests, PACT was positioned so that the compaction surface was parallel with the simulant and lowered in 0.1 mm increments until the load cell read 74 N +/- 10% which is equivalent to 7 kPa. The single-mass vibration motor was activated, and it was observed that the force measured by the loadcell decreased.

In spot compaction tests, PACT was then continually lowered in 0.1 mm increments to maintain the 74 N load (+/- 10%) for 180 seconds. A static load was not ever reached. It should be noted that the in-vacuum spot compaction testing executed four tests in independent areas of the bin in a single simulant preparation cycle whereas ambient testing reset the simulant for each test.

In raster compaction tests, PACT was linearly translated 300 mm along the X-axis thus compacting the regolith bed. The scoop was then lifted and translated linearly in Y and lowered

again until the force value was met. It was then translated backwards along the X-axis to the starting position compressing an overlapping line. This process was completed until a rectangular bed of 300 mm x 200 mm was compacted. In ambient raster compaction testing, only a single X-axis translation pass was made.

g. Geotechnical Tools

Three physical data collection tools were used to collect density values: a core sampler, a cone penetrometer, and a pocket penetrometer.

For the core sampler (Figure 13), a thin-walled tube of 60 mm inner diameter and 25 mm depth was pressed into the regolith to extract a cylinder of regolith un-disturbed, with a known volume. This cylinder of regolith is then weighed, and a density value is calculated.

Figure 13. 60mm diameter 25 mm depth core sampler. Lid is used during transport to the scale and is installed prior to core excavation from the simulant surface.

The cone penetrometer (Figure 14) that was used was a Humbolt HS-4210 with a 60° cone head with a 1.5 cm^2 area. The cone penetrometer is slowly lowered down into the regolith surface (about 1-2 cm/s) and force readings are called out by the operator at 51, 76, 102, 127, 152, 178, and 203 mm depths (2, 3, 4, 5, 6, 7, and 8 inches). For analysis, sets of three cone penetrometer readings are averaged together to create an upper (51-102 mm), middle (102-152 mm), and lower (152-203 mm) regions. These regions are shown graphically in Figure 15.

The pocket penetrometer that was used was a Humbolt H-4205 with a 20 mm diameter foot for compacted regions and a custom 60 mm diameter foot for uncompacted regolith regions. Both feet are 15 mm in thickness and are pressed down into the regolith until the top surface of the foot is flush with the regolith.

Figure 14. Cone penetrometer (left) and pocket penetrometer (right).

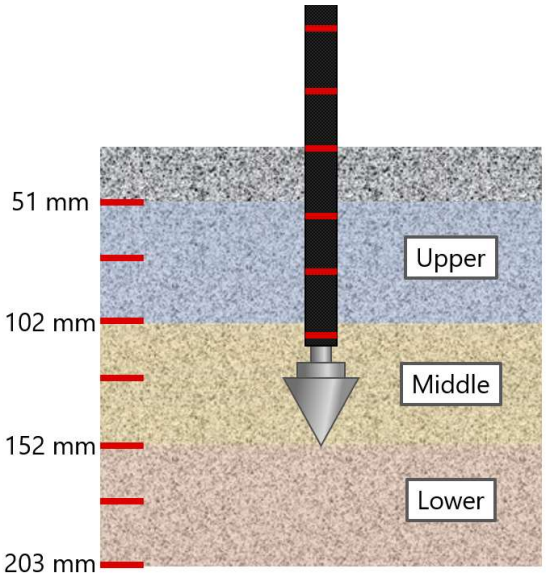

Figure 15. Cone penetrometer measurement readings.

h. Data Collection Process

Density readings (raster and spot) and settlement (spot only) were collected by operators before and after compaction. Figure 16 shows the layout of a Spot compaction test and the location of sample collection sites. The compaction surface is visible as a square region in the center of the test area. Circular patches are locations of pocket penetrometer readings. Cone penetrometer locations appear as smaller circular disturbances in the BP-1. The "C103i1" written into the BP-1 was the internal test numbering system and was written into the soil after compaction to improve image archiving and referencing. Blue sites are performed prior to compaction, red sites are performed after compaction. Sites 1, 2, 3, 4, and 5 include a cone penetrometer and pocket penetrometer reading. Sites 6 and 7 were only cone penetrometer reading locations. Sites 6 and 7 were to verify if compaction of regolith outside of the compaction zone occurred.

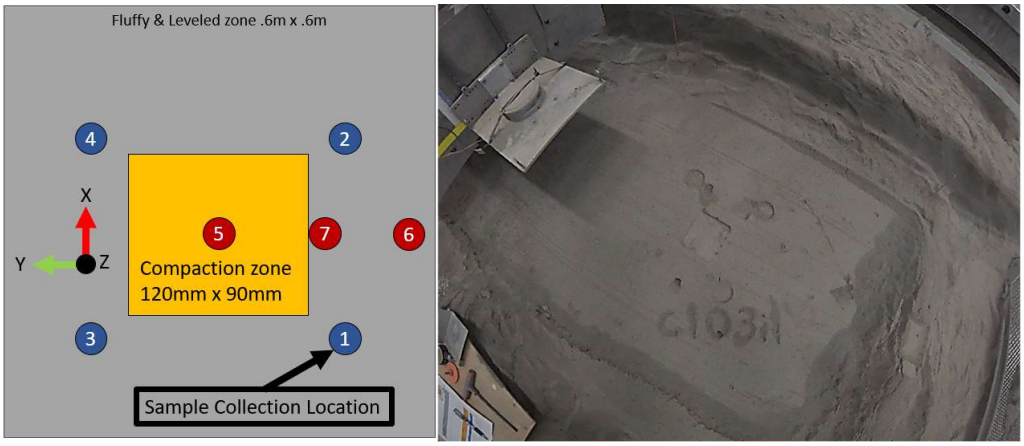

Figure 16. BP-1 Spot compaction measurement location layout (left) and post compaction test area after measurements (right).

Figure 17 shows the layout of Raster compaction testing for BP-1 and the sample collection sites. In BP-1 raster tests, sites 1, 2, 3, and 4 were done prior to compaction and cone penetrometer and pocket penetrometer data was collected. At sites 5, 6, 7, 8, 9 and 10 a cone penetrometer reading was taken. At sites 5, 6, and 7 a core sample was collected. The compaction surface is visible as a rectangular region in the center of the test area. While difficult to see in the image, circular patches are locations of pocket penetrometer readings. Cone penetrometer locations appear as smaller circular disturbances in the BP-1. The "C19i1" written into the BP-1 was the internal test numbering system and was written into the soil after compaction to improve image archiving and referencing.

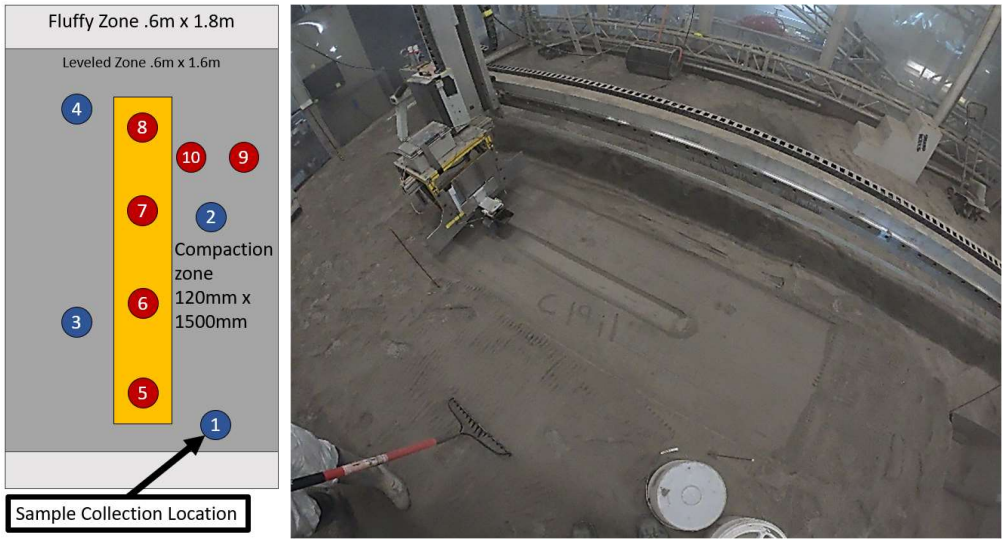

Figure 17. BP-1 raster compaction measurement location layout (left) and post compaction test area after measurements (right).

For LHS-1 testing the data collection sites were the same but for sites inside the compacted region a pocket penetrometer reading, and core sample were taken rather than a cone penetrometer reading. This was to have core sample data to compare against the previously done in-vacuum testing that was exclusively core sample readings. A single test using the dual-mass motor was performed in LHS-1. For that test rather than taking a core sample of the spot compaction site, a cone penetrometer reading was substituted. This was to better compare that test to the BP-1 spot compaction tests. Figure 18 shows the LHS-1 and Raster data collection results with compaction imprints.

Figure 18. LHS-1 Spot (left) and Raster (right) compaction final test area surface.

6. Compaction Testing Results

a. Peak Applied Pressure

The Z-axis load cell readings were utilized to estimate the peak compaction pressure which is produced from the static compaction pressure applied via weights combined with a dynamic pressure imparted by the vibratory motor (if vibration was used during the test). For Spot compaction tests, static weight plus dynamic vibratory force creates the peak applied pressure. For raster compaction tests, static compaction pressure is zero and only the dynamic vibratory force is producing peak applied pressures. Table 3 shows the various calculated or assumed peak pressures for each configuration of the PACT system (compaction motion, frequency of dual-mass motor, and static pressure applied via weights). The single-mass motor peak pressures are not included as the single-mass motor operates in the X-Y plane and so peak pressures are assumed to equal the applied static pressure of a given test.

For raster compaction tests at 0 kPa static pressure, measured peak pressures were from 3.45 to 3.9 kPa. Changes in frequency setpoint of the vibratory motor did not have a significant impact on applied peak pressure.

For spot compaction tests at 7 kPa static pressure the Z-axis load cell readings successfully were used to estimate this peak pressure. For spot compaction tests at 7 kPa the peak applied pressure was estimated from 6.8 to 11.3 kPa.

Two accuracy concerns were witnessed with the pressure measurement load cells. In spot compaction at 7kPa static pressure, in some cases, the peak pressure appeared lower than the known static pressure applied by the weights on the system. This indicates a substantial degree of uncertainty in peak pressure measurements. This may be due to the accuracy of the load cells at this lower weight range (full range is 0 to 92.6 kPa). In spot compaction tests at the greater, 70 kPa, static pressure loads the load cell data was unable to provide reliable peak loading information. Load was seen in the Z, X, and Y axis of the load cell indicating that flex of the load-cell was occurring in all directions. There was no confident failure mode identified. Though the misreading may be due to the high static load weights flexing the system causing a misalignment and possibly preload in the load cell assembly. For 70 kPa tests, the added pressure due to vibratory actuation is assumed to be negligible and these tests are assumed to be at a static pressure of 70 kPa.

Table 3. Calculated peak pressure for each compactor configuration.

Compaction Motion	Frequency of Dual-Mass Motor (Hz)	Static Pressure (kPa)	Calculated Peak Pressure (kPa)
Spot	45	7	9.75-11.25
Spot	71	7	6.75-10.75
Spot	0	7	7
Spot	0/45/71	70	70 (not measured, assumed)
Raster	45	0	3.45
Raster	71	0	3.5-3.9

b. Effect of Surface Contact Time

BP-1 Spot compaction 0 Hz (no vibration), 45 Hz, and 71 Hz tests at 7 kPa static force compaction data is presented in Figure 19. The X-axis is the applied compaction pressure via PACT onto the BP-1. This is read as a reaction force into the load-cells on PACT. Density is calculated from the pocket penetrometer pressure reading using the equation outlined in *Appendix A: Estimation of Bulk Density with Pocket Penetrometer Tests (PPT)*. Of the contact times explored within this test set, the 45 Hz spot compaction tests at 7 kPa were only able to achieve 80% relative density with the longest contact times (180 seconds). This suggests a week correlation between contact time and compacted density may exist under these conditions. For 71 Hz, 7 kPa static pressure tests all surface contact times were effective and there does not appear to be a clear improvement in surface compaction between 30 and 180 second tests. This indicates that 30 seconds of contact time may be adequate to achieve maximum surface compaction for the 71 Hz, 7 kPa compaction case with PACT.

All 70 kPa static pressure spot tests were performed at 180 second surface contact time and so an effect of surface contact time at this high pressure cannot be derived.

Raster compaction testing showed similar results with no appreciable difference in results for both surface pocket penetrometer readings and at depth cone penetrometer readings for various surface contact times.

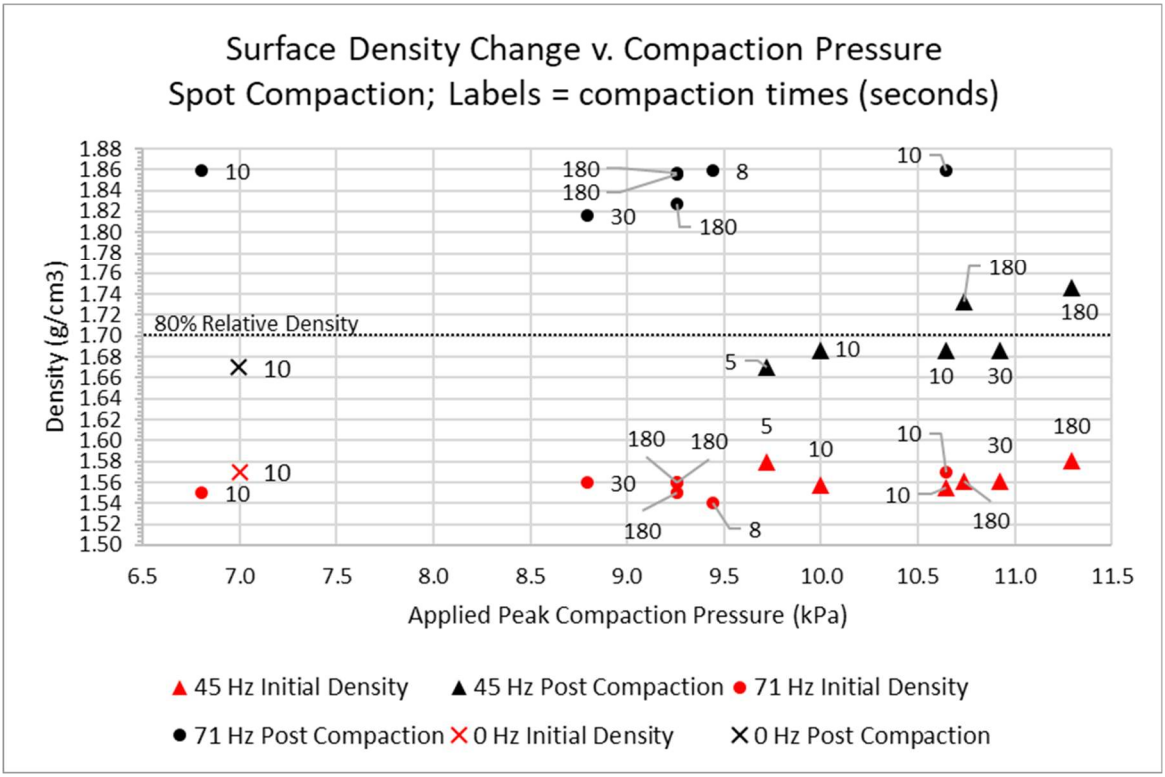

Figure 19. Spot compaction - surface density of BP-1 changes with compaction pressure.

Figure 20 and Figure 21 show the cone penetrometer measurements for spot compaction tests at 45 and 71 Hz and 7 kPa static pressure. In both 45 and 71 Hz configurations there does not appear to be a strong relationship between surface contact time and cone penetrometer force at the

upper, middle, or lower reading zones. There appears to be the greatest increase in cone penetrometer readings for the shorter 8 and 10 second tests at 71 Hz, but the data set is limited, and the manually operated cone penetrometer has a relatively high degree of uncertainty. High force readings in the lower zone (152-203 mm) may be due to the bottom of the prepared regolith area producing higher readings on the cone penetrometer.

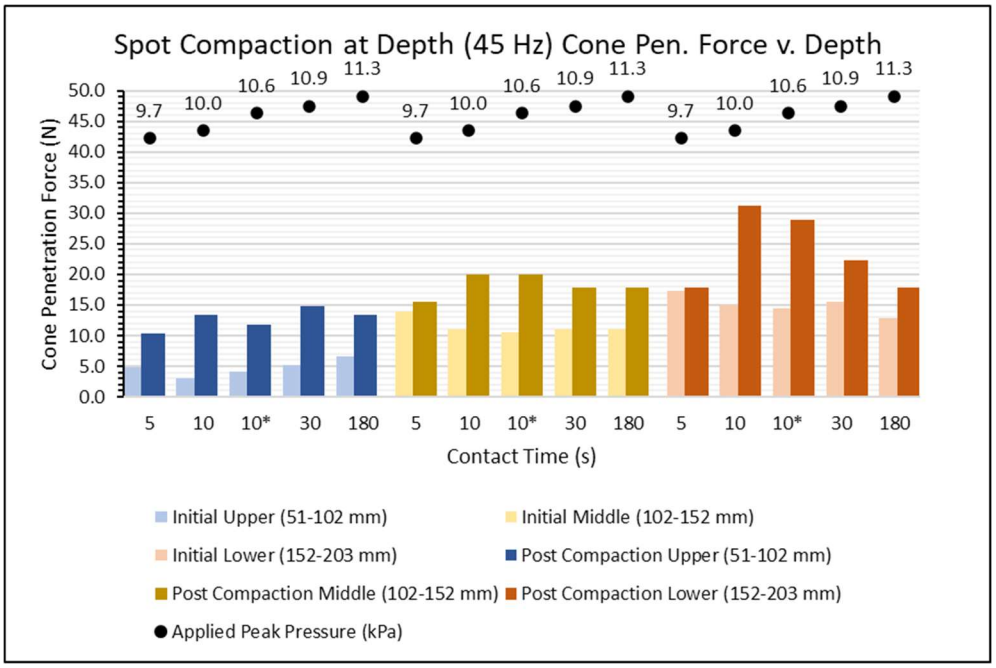

Figure 20. Cone penetrometer force measurements for 45 Hz, 7 kPa spot compaction tests in BP-1 (asterisks added to differentiate results for tests with like contact times).

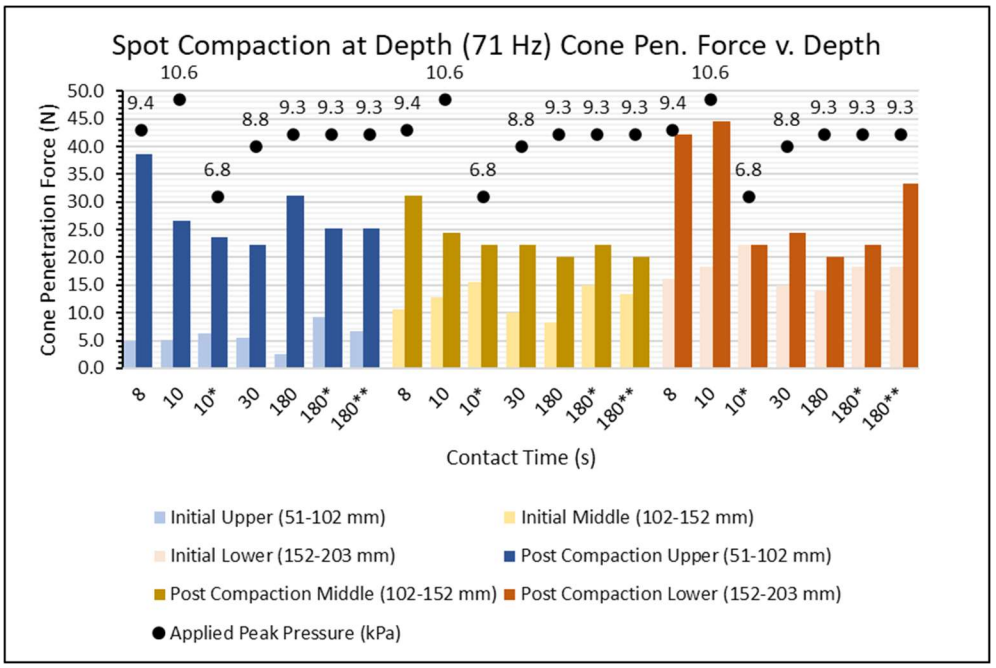

Figure 21. Cone penetrometer force measurements for 71 Hz, 7 kPa spot compaction tests in BP-1 (asterisks added to differentiate results for tests with like contact times).

c. Displacement Depth During Spot Compaction

Figure 22 displays the achieved displacement depth of the compaction plate into the BP-1 regolith at a lower static load (7 kPa) at the frequencies 45 Hz and 71 Hz.

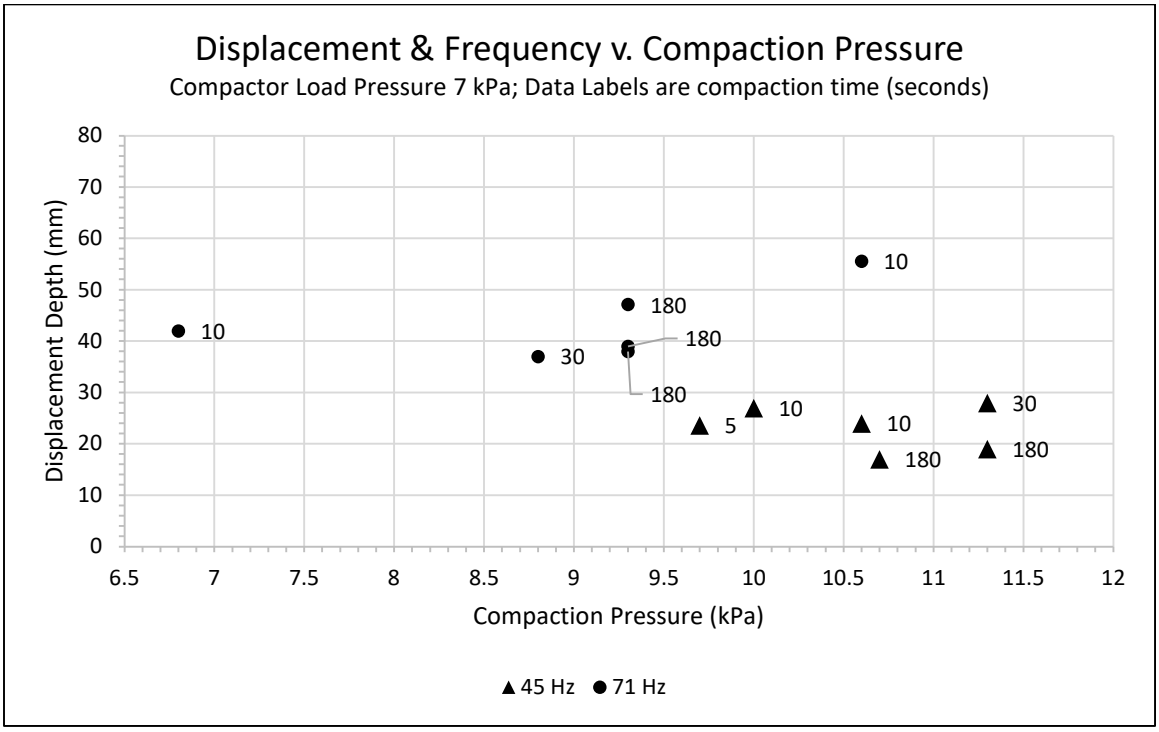

Figure 22. Displacement depth for vibratory spot compaction of BP-1 at 45 Hz and 71 Hz.

At 45 Hz, the vibrating compacting plate achieved a displacement depth that seems independent to the duration of the compaction time, ranging from 5 to 180 seconds.

At 71 Hz, the displacement depth is between 35 to 115% higher than that achieved at 45 Hz under similar compaction pressure, indicating a more efficient transfer of energy into the regolith to achieve compaction. 180 seconds does not appear to have an increase in displacement depth over the 71 Hz, 10 second tests. This indicates that the system may be achieving its maximum displacement depths within the first 10 to 30 seconds of compaction and there are diminishing returns to additional compaction contact times.

Figure 23 shows the displacement depth average ("x"), max and minimum (whiskers), and upper and lower quartile (box) for each spot compaction test configuration, including the 70 kPa static pressure tests. In both the 0 Hz and 71 Hz cases, the 70 kPa tests show an increase in settlement over the 7 kPa tests.

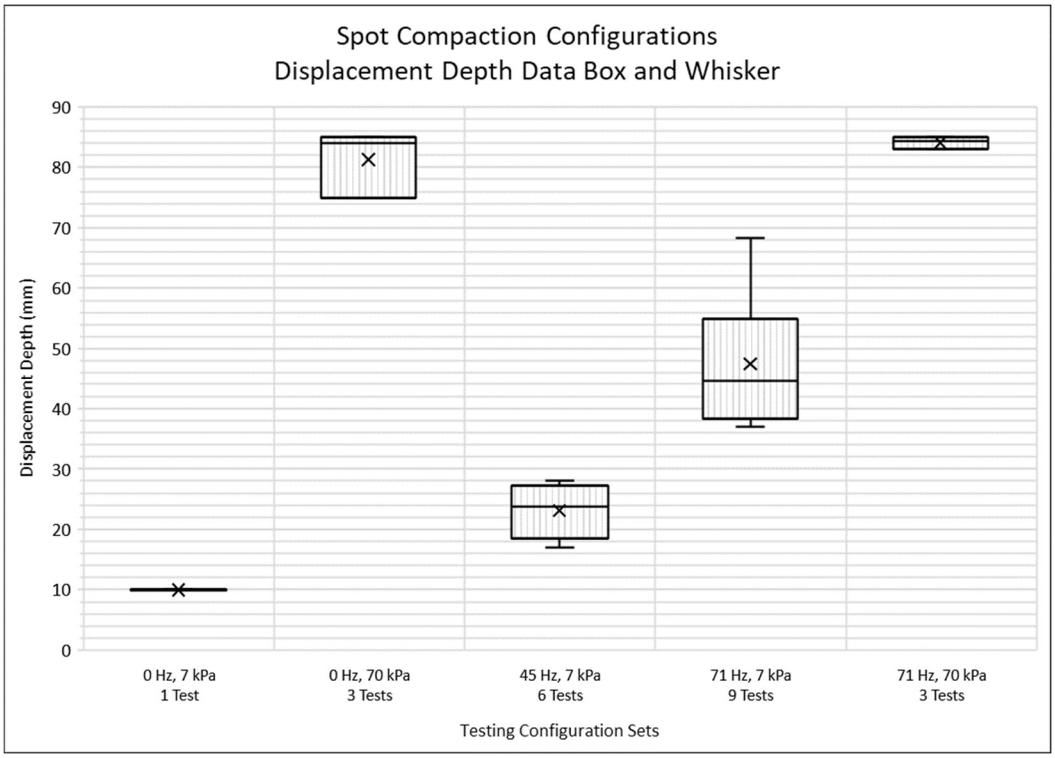

Figure 23. Box and whisker plot of BP-1 Spot compaction settlement travel.

d. Effect of Frequency and Static Pressure at Depth

Figure 24 shows a summary of cone penetrometer data from spot compaction tests as a box and whisker plot. The average ("x"), max and minimum (whiskers), and upper and lower quartile (box) are shown for each configuration. Surface contact times are ignored for this plot.

71 Hz tests show higher cone penetrometer measurements on average when compared to 45 Hz and 0 Hz. This indicates that 71 Hz does produce an appreciable improvement to compaction when compared to other frequencies at lower static compaction pressures.

When the compaction pressure is high, such as 70 kPa, there does not appear to be a strong relationship between vibratory frequency and compaction at depth. At 70 kPa static pressure, the middle and lower cone penetrometer readings are within the same range of results for 0 and 71 Hz tests. It is likely the static pressure is high enough to make the dynamic vibratory force negligible in the overall peak applied pressure.

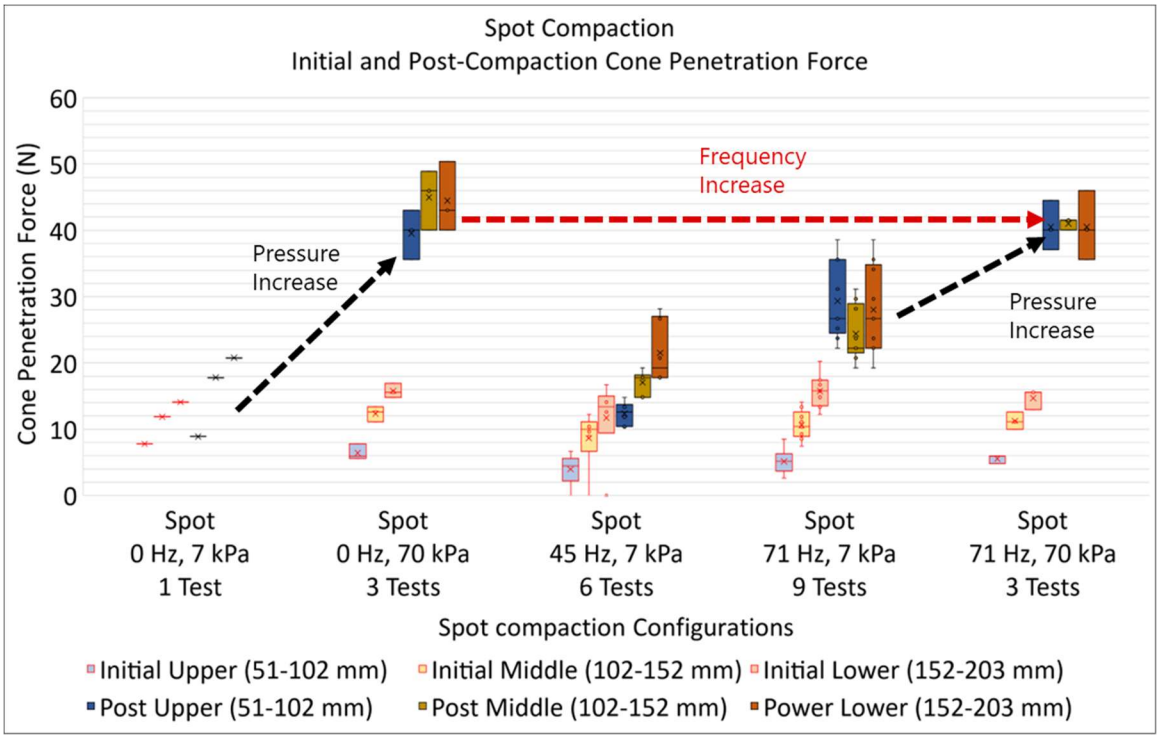

Figure 24. Spot compaction cone penetrometer force measurement data box and whisker for each PACT configuration.

e. Effectiveness of Spot vs. Raster Compaction

To compare the relative effectiveness of spot compaction to raster compaction a summary box and whisker plot was generated. This plot, Figure 25, was developed by calculating the percent change in measured pocket penetrometer surface density and cone penetrometer force readings from the initial prepared BP-1 to the post-compaction BP-1. Note the Percent change for each measurement group is normalized from 0 to 1 with 1 being the highest percent change in value.

While this method of processing the data and plotting does not show absolute values for any given test, it can be effective as providing a relative comparison between each of the configurations of the PACT system. Tests that achieved 1 on the normalized y-axis achieved the highest recorded change for that given measurement sub-set.

Spot compaction appears to outperform raster compaction at surface bulk density and cone penetrometer force measurements in all cases except when operating at 71 Hz.

This chart also demonstrates the average improvement in compaction as spot compaction frequency is increased from 45 Hz to 71 Hz and static compaction pressure is increased from 7 kPa to 70 kPa.

Raster compaction at 45 Hz and 5mm pass depth showed a higher-than-expected surface density. With only one test at this frequency, it is difficult to determine if this is a result of the compaction parameter configuration or an issue with pocket penetrometer readings for that test.

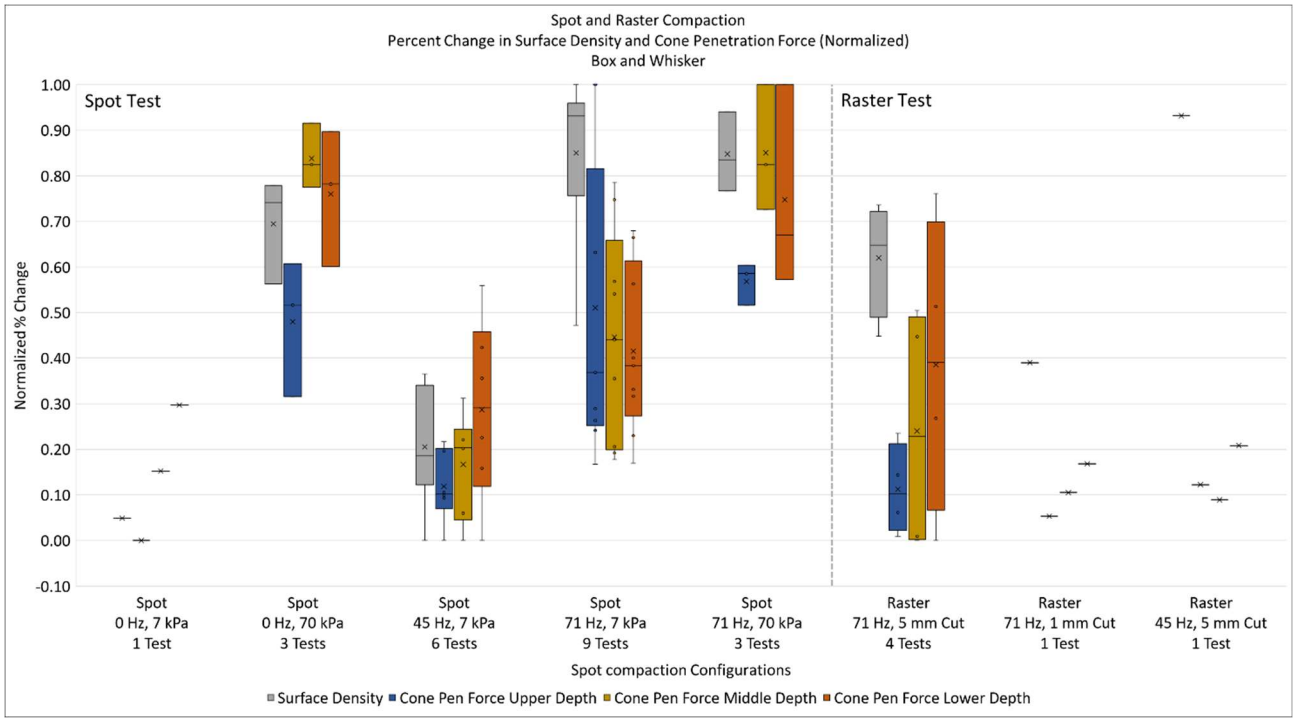

Figure 25. Box and Whisker comparison of BP-1 spot compaction to raster compaction motion by comparing the percent change in measurements from before and after compaction.

f. Raster Pass Depth Impact on Compaction at Depth

While a single test of raster compaction at a reduced 1 mm cut depth was performed to compare against 5 mm testing, the range of test results from raster testing showed a broad range of measurements (as shown in the percent change normalized chart, Figure 25). While it appears, based on the one test, that 1 mm raster passes are less effective than the average results for 5 mm passes, no significant conclusion can be made at this time without additional pass depth testing.

g. Spot Compaction LHS-1 vs. BP-1 in Ambient Conditions

Figure 26 presents the data for spot compaction with the dual-mass motor in LHS-1 v. BP-1 at 71 Hz for 180 s in ambient conditions. The data is provided in terms of relative density to allow for comparison across the two simulants. The calculations presented in *Appendix B: Relative Density Calculations* were used to convert absolute density to relative density. An applied compaction pressure (static pressure plus vibratory motor applied pressure) of 6.8 kPa increases the relative density of LHS-1 from 54% to 84%. In BP-1, an applied compaction pressure of 9.3 kPa increases the relative density from 60% to 99%. The compaction process resulted in a 30% increase in relative density in LHS-1 and a 39% increase in BP-1. BP-1 compaction tests experience a 2.5 kPa higher applied pressure compared to the LHS-1 test. Based on these initial and limited testing results, the two simulants appear to respond to the compaction process very similarly. It is also shown that in this configuration, the PACT system is successful in achieving 80% relative density in both simulant types.

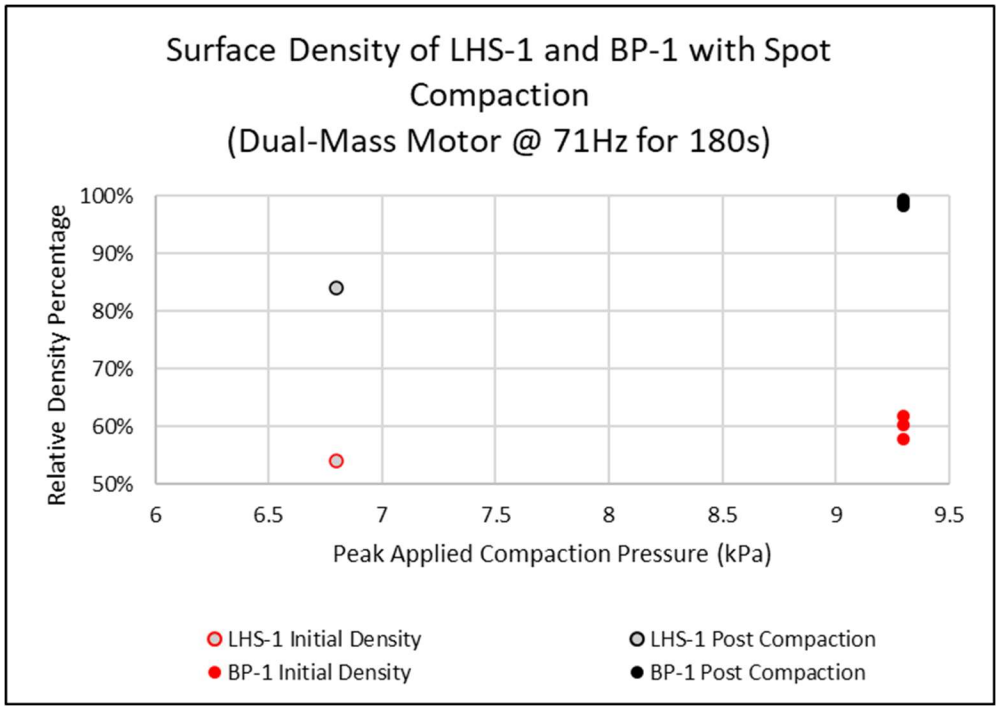

Figure 26. Comparison of surface density pre and post compaction of LHS-1 and BP-1 using the dual-mass motor. Change in density is similar between simulants.

h. LHS-1 Compaction in Ambient vs Vacuum

Spot Compaction

Density data from core sampling for spot compaction in LHS-1 in ambient and vacuum conditions are presented in Figure 27. Ambient compaction yielded an average density of 1.73 g/cm^3 and compaction in vacuum resulted in an average of 1.77 g/cm^3. These measurements were taking directly using the 60 mm diameter x 25 mm deep core sampling tool. Core samples for vacuum tests were performed after venting the vacuum chamber to ambient conditions. Testing in ambient and in vacuum appear to have similar results, though the vacuum condition results show a slightly higher average final surface bulk density.

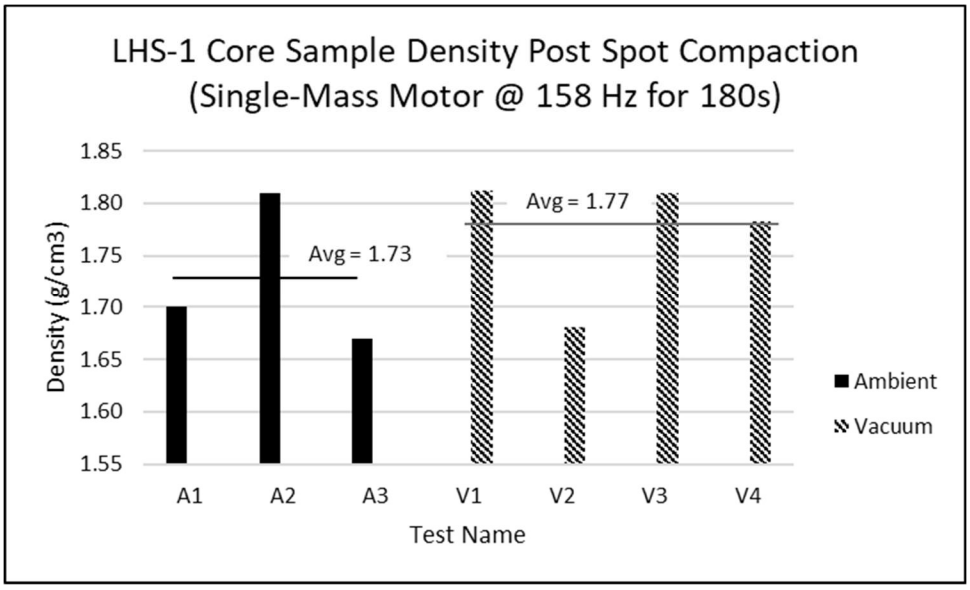

Figure 27. LHS-1 post compaction core sample densities after spot compaction with the single-mass motor both in ambient and in vacuum. Results show comparable compaction densities.

The LHS-1 simulant settlement depth in response to compaction in ambient and vacuum was similar as well. Settlement in ambient was measured and ranged between 10 and 32 mm with an average of 20 mm. Settlement in vacuum was determined by photogrammetry of video footage to be approximately 10 mm.

It should be noted that the four vacuum tests were executed in separate areas of the LHS-1 bin in a single simulant setup cycle, but in ambient testing, the simulant was reset for each test. Additionally, the LHS-1 could have experienced changes in initial and final densities during the pump-down and return to atmospheric pressure phases that were not experienced during ambient testing. These differences could have influenced the density and settlement depth measurements, though it is not clear if this is the case or if it would have tended to increase or decrease the value of the measurements.

Raster Compaction

Density data from core sampling for raster compaction in LHS-1 in ambient and vacuum conditions are presented in Figure 28. Ambient compaction yielded an average density of 1.74 g/cm^3 and compaction in vacuum resulted in an average of 1.69 g/cm^3. Like spot compaction testing, ambient and in-vacuum testing appear to have similar final results though the average surface bulk density in ambient testing cases is higher than that of in-vacuum tests.

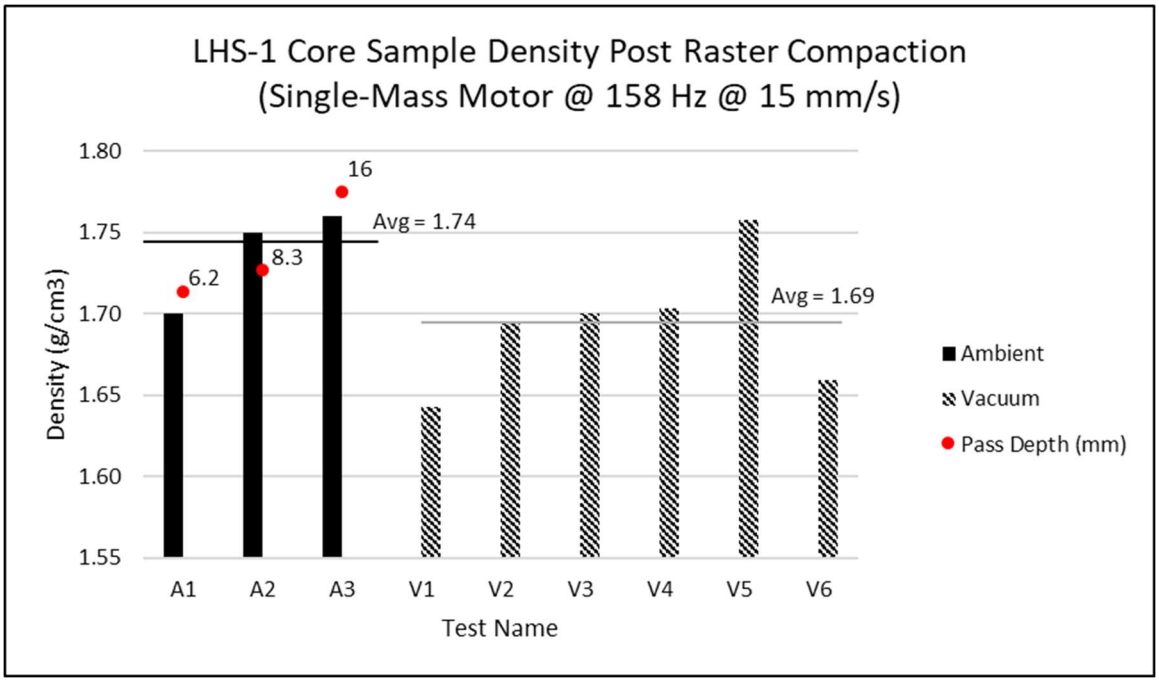

Figure 28. LHS-1 post compaction core sample densities after raster compaction with the single-mass motor both in ambient and in vacuum. Results show comparable compaction densities.

It should be noted that ambient tests were a single pass of raster compaction in the x-axis for 300 mm. The vacuum test cases performed three rows of partially overlapping raster compaction resulting in a 300 mm long by 200 mm wide area. In both ambient and in-vacuum tests each row was compacted using a single raster pass. The pass height was set by lowering the compactor into the LHS-1 simulant to achieve 7 kPa pressure on the compactor, fixing z-axis to that height, then moving in the X-axis. These pass depths were 6.2, 8.3, and 16 mm for A1, A2, and A3 respectively. Tests performed in vacuum did not record the pass depth but were performed conducting the same method. All the core samples were taken from the compacted area once the test area was brought back to ambient pressure. Ambient testing included simulant preparation with the same method as used in the vacuum testing followed by single linear passes for each test configuration. It should be noted that the LHS-1 could have experienced changes in initial and final densities during the pump-down and return to atmospheric pressure sequence which did not happen during ambient testing. If these changes occurred, the resulting differences in regolith behavior could have influenced the density measurements, but whether these would result in increased or decreased density values is not known.

7. Conclusions

a. Results

The testing of the PACT plate compaction system showed effective compaction (80%RD or greater) by utilizing a spot compaction motion method making use of a small-scale arm end effector system. This system could be reasonably powered on a technology demonstration mission such as a Commercial Lunar Payload Services (CLPS) lander. An example of this is the Intuitive

Machines Lunar Access vehicle which offers 5, 12, and 28 VDC and up to 200 W of power to payloads [4].

Some initial optimization observations were found as a result of this testing campaign, including:

1. 7 kPa of static compaction pressure and a vibratory force of approximately 3.5-4.0 kPa is adequate to achieve 80%RD at the surface, though more compaction pressure may be needed for adequate subsurface compaction levels.
2. Surface contact times greater than 30 seconds have significant diminishing returns on for PACT compaction in the 71 Hz case.
3. The PACT configuration utilizing the dual-mass motor at 71 Hz is more effective at subsurface compaction than the 45 Hz configuration.
4. A raster style compaction method that does not utilize static compaction pressure is not as effective as a spot compaction motion path.
5. BP-1 and LHS-1 under plate compaction appear to have similar density changes for spot compaction.
6. LHS-1 in vacuum and in ambient conditions appear to behave similar under plate compaction.

While these are initial observations from testing, it should be noted that in some cases the number of repeat tests performed was limited and additional work is required to further optimize the compaction concept of operation, mission time, and needed power input. This testing may use ambient condition testing to further refine before more relevant vacuum testing is performed.

Additionally, preparing simulants to below 50%RD is very challenging at a large enough volume to perform compaction testing at scale. Further work to quantify the sensitivity of a compactor system to initial starting density would improve confidence a system can operate over a broad range of starting conditions.

b. Need for Variable Frequency in a Lunar TRL 6+ System

Many factors can impact the effectiveness of a plate compactor system. While this paper explores a set of parameters, it is under specific environmental conditions and two with lunar simulants. The lunar surface will vary in several ways including the regolith mechanical properties, electrostatic forces, chemical makeup, and the force of gravity is $1/6^{th}$ that of Earth. For example, in Azema et. al [5] demonstrated by modeling that motion of particles under vibration (in this case, horizontal and not plate compaction) is affected by gravity.

The PACT development team recommends that further development on a plate compactor system include the capability to vary vibratory frequency and amplitude (both force and displacement) to allow a lunar mission to tune compaction parameters in-situ.

Additionally, lunar gravity testing of compaction via a parabolic flight demonstration could reduce risk and improve compactor design efficiency by reducing the possible frequency and amplitude window.

8. References

[1] E. Bell, E. Jose Bidot, N. J. Gelino and P. R. Mueller, "Multifunctional End Effector for Regolith Construction, Acquisition, and Transfer (MEERCAT)," in *ASCE Earth and Space*, Miami, 2024.

[2] J. Schuler, A. Nick, K. Leucht, A. Langton and D. Smith, "ISRU Pilot Excavator: Bucket Drum Scaling Experimental Results," in *ASCE Earth & Space*, Miami, 2022.

[3] G. J. Nathan, E. A. Bell and M. W. Nugent, "Development of the Advanced Regolith Ground Operations (ARGO) Test Bed - A Robotic Excavation and Construction Test Facility with Simulated Lunar Environments," in *ASCEND*, Las Vegas, NV, 2023.

[4] Intuitive Machines, LLC, "Lunar Access Services User's Guide V.1.5," in *www.Intuitivemachines.com/rideshare*, 2025.

[5] E. Azema, F. Radjai, R. Peyroux, F. Dubois and G. Saussine, "Vibrational dynamics of 3D granular media composed," in *IX Congreso de Geotecnia, Sociedad Colombiana de Geotechnica*, Bogotà, Colombia, 2008.

[6] M. C. Amacher and K. P. O'Neill, "Assessing Soil Compaction on Forest Inventory & Analysis Phase 3 Field Plots Using a Pocket Penetrometer," US Department of Agriculture, Forest Service, Rocky Mountain Research Station, 2004.

[7] F. Musavi, E. Abdi, S. Ghalandarayeshi and D. S. Page-Dumroese, "Modeling Unconfinded Compressive Strength of Fine-Grained Soiles: Application of Pocket Penetrometer for Predicting Soil Strength," *Catena,* no. 104890, p. 196, 2021.

[8] E. Suescun-Florez, S. Roslyakov, M. Iskander and M. Baamer, "Geotechnical Properties of BP-1 Lunar Regolith Simulant," *Journal of Aerospace Engineering,* vol. 28, no. 5, p. 04014124, 2015.

[9] ASTM Standard D4254, *Standard Test Methods for Minimum Index Density and Unit Weight of Soils and Calculation of Relative Density,* West Conshohocken, PA: ASTM International, 2016.

[10] J. J. Kolbuszewski, "An Experimental Study of the Maximum and Minimum Porosities of Sands," in *International Conference on Soil Mechanics and Foundation Engineering Vol. 1.*, Gebr, Keesmaat, Haarlem, The Netherlands, 1948.

[11] J. M. Long-Fox, Z. A. Landsman, P. B. Easter, C. A. Millwater and D. T. Britt, "Geomechanical Properties of Lunar Regolith Simulants LHS-1 and LMS-1," *Advances in Space Research,* vol. 71, no. 12, pp. 5400-5412, 2023.

9. Appendix A: Estimation of Bulk Density with Pocket Penetrometer Tests (PPT)

a. Background

Pocket Penetrometer Background

A pocket penetrometer measures the pressure exerted by the soil on the tip of the device when the user applies sufficient force into the soil to penetrate to the target depth. The pressure measured (in kg/cm2) is converted to kPa. This allows soil engineers to find the unconfined compressive strength (UCS) of a given soil through correspondence tables. It is important to note that the pocket penetrometer instrument is only a surface measuring device and is not used to investigate how the soil changes with depth. The UCS is also a measure of the degree of compaction of a given soil. The soil classification is important not only to find the UCS but also to determine applicability of the measurement. Recent research shows that pocket penetrometers can be used to determine soil compression strengths in the field and determine the degree of compaction [6] [7]. which is linked to soil density. Pocket penetrometers are widely used in cohesive soils with wide range of moisture content. They are not applicable for use in sand unless the classification is that of an angular sand. This grain property provides the sand an apparent cohesion because of high inter-particle friction which is also the case in lunar regolith simulant materials. For this reason, the pocket penetrometer may provide useful data in lunar regolith research.

In the case of BP-1 and LHS-1 regolith simulants, the correspondence between pocket penetrometer pressure and UCS has not yet been established. Instead, we established the relationship between independently measured bulk density and pocket penetrometer pressure readings that are a measure of the regolith compressive strength in the test field.

Pocket Penetrometer Use in PACT Testing

A Humbolt H-4205 pocket penetrometer was used to record surface density with a 20-mm diameter foot and a custom 60 mm diameter foot. The 60 mm foot was preferred for low-bulk densities for better reading range on the pocket penetrometer's dial. The H-4205 provides a reading in kg of force imparted by the user to press the cylindrical foot 15 mm into the soil, so that the soil surface is flush with the top of the foot. This kg of force can be converted to a pressure applied to the surface based on the area of the foot used in the test. The use of the pocket penetrometer as a tool to estimate the bulk density of the regolith at the surface requires that the kg-force or pressure measurement must correspond to a measured bulk density value for the selected regolith simulant (in this case BP-1 and LHS-1). This correspondence was established by performing a series of known-density measurements with the pocket penetrometer with both the 20-mm and 60-mm foot to cover the range of expected bulk densities. The testing and final results are outlined in this section. Figure 30 shows this correspondence in which the pressure readings for both foot diameters (20 and 60 mm) are confirmed to follow the same relationship with bulk density within the known uncertainty of pocket penetrometer readings typically estimated between 20 to 40%. A polynomial equation provides an adequate fit within the range of pressure measurements.

b. BP-1 Test Procedure

A Humbolt Split Compaction mold with a height of 155.15 mm and a diameter of 151.93 mm (Figure 29) was used as a container and partially filled with regolith. To achieve low bulk density ($\leq$1.55 g/cm^3), the mold was filled slowly by sprinkling in BP-1. To avoid disturbing the top surface density, the surface was not sheared or leveled. Instead, the height of the surface was measured at four equidistant points and an average height was taken.

For higher densities (>1.55 g/cm^3) the mold was filled in one third sections via sprinkling. Each section is then tamped by placing an approximately 10 mm thick aluminum plate cover on top of the regolith surface and impacting it using a Humbolt Aggregate Tamper. The drop mass on the aggregate tamper is 4.2 kg and the total mass of the tamper, including the drop mass, is 8.3 kg. To vary the compaction level, the mass on the tamper was raised to specific heights, higher for more tamping impact. Multiple impacts from this height were also performed to increase compaction level for a given sample. The heights and number of impacts are recorded in Table 4. After tamping, the Pocket Penetrometer was used to collect a kg force reading that was converted to a pressure.

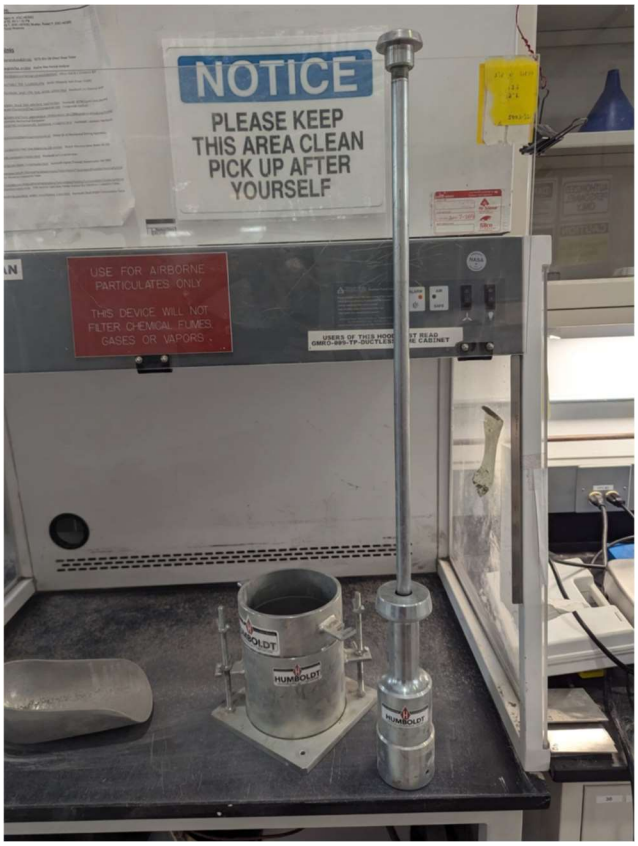

Figure 29. Humbolt Split Compaction Mold and Humbolt Aggregate Tamper.

For some later tests at higher densities, the mold height was increased using an additional cylindrical section, filled high, tamped, the additional section was removed, and a screed was used to level the surface to a height 155.15 mm before the pocket penetrometer was used and the sample was weighed to improve workflow and height accuracy.

To maintain consistency and prevent fragmentation of regolith, each test was performed with a new batch of BP-1 sourced from the Big Bin. This testing was performed for both the 20 mm and 60 mm pocket penetrometer feet.

c. BP-1 Density - Compression Strength Correlation

Table 4 shows the results of the regolith compression strength-surface bulk density correlation measurements plotted as bulk density as a function of pocket penetrometer pressure (Figure 30). There appears to be a consistent trend in the relationship between surface bearing pressure and bulk density and the data collected follows the trend well. The curve fit used is a second order polynomial with a strong fit to the data. While the trendline equation follows the data well, there is not data for pressure readings over 45 kPa or bulk densities greater than 1.75 g/cm^3. It appears that without significant additional force, a density over 1.75 g/cm^3 is not possible using this testing setup. This is consistent with previous BP-1 density testing that achieved a maximum density of 1.75 g/cm^3 using ASTM D4253 [8]. This may be that to achieve higher densities, facture of the regolith particles may be required.

Table 4. BP-1 Pocket Penetrometer correspondence tests.

Pocket Pen Head Size (mm)	Tamper Release Height (mm)	# Tamping Impacts	Mass of Regolith (kg)	Height (mm)	Regolith Volume (cm^3)	Pocket Pen Pressure (kPa)	BP-1 Bulk Density (g/cm^3)
20	No Tamping	0	4.15	155.15	2813	0.0	1.48
20	No Tamping	0	4.32	155.15	2813	1.6	1.53
20	No Tamping	0	4.47	155.15	2813	12.5	1.59
20	5.00	6	4.47	147.71	2678	18.8	1.67
20	5.00	4	4.46	148.65	2695	15.7	1.65
20	10.14	6	4.37	148.55	2693	19.8	1.62
20	20.95	7	4.54	148.65	2695	25.7	1.68
20	25.17	6	4.61	150.57	2730	22.0	1.69
20	25.17	11	4.92	155.15	2813	39.2	1.75
20	30.15	4	4.85	155.15	2813	42.4	1.72
60	No Tamping	0	4.15	151.76	2751	2.4	1.51
60	No Tamping	0	4.25	155.15	2813	2.7	1.51
60	No Tamping	0	4.34	155.15	2813	6.7	1.54
60	No Tamping	0	4.37	155.15	2813	5.8	1.55
60	No Tamping	0	4.28	152.62	2767	6.8	1.55
60	No Tamping	0	4.21	148.46	2692	6.6	1.57
60	No Tamping	0	4.32	155.15	2813	4.9	1.54
60	No Tamping	0	4.64	155.70	2823	21.0	1.64
60	No Tamping	0	4.59	155.15	2813	21.0	1.63
60	No Tamping	0	4.47	155.15	2813	10.5	1.59

60	4.89	6	4.74	155.15	2813	34.9	1.69
60	4.89	3	4.74	155.15	2813	35.3	1.69
60	5.00	4	4.62	153.17	2777	28.3	1.66
60	5.00	2	4.46	149.01	2701	21.3	1.65
60	8.37	6	4.64	155.15	2813	30.0	1.65
60	18.28	9	4.81	155.15	2813	38.1	1.71

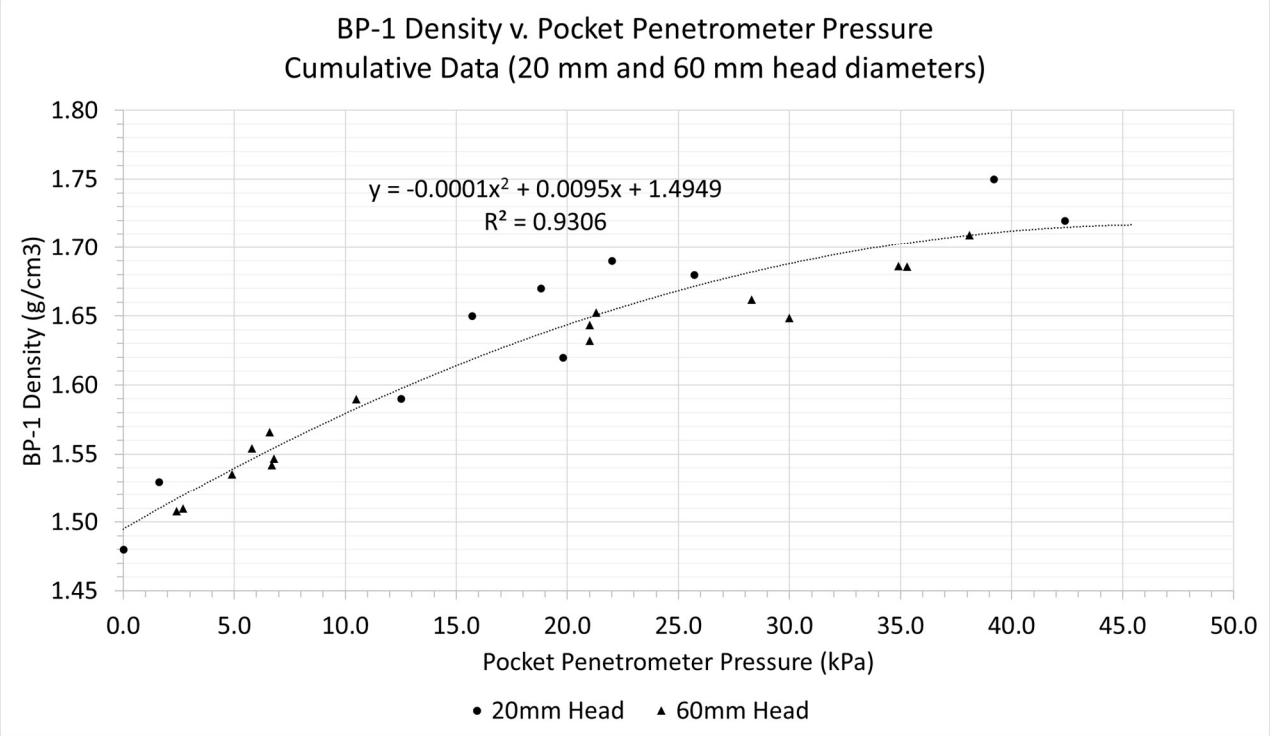

Figure 30. BP-1 density v. pocket penetrometer pressure correlation (limited range).

d. BP-1 Range Limitations and Solutions

While the results of the density-PPT correlation testing showed a clear trend, the compaction method could not achieve densities reliably over 1.72 g/cm^3 which corresponds to a pocket penetrometer reading of 42.4 kPa. Consequently, the polynomial trendline developed cannot be used for estimating the surface bulk density above these values. Figure 31 shows where the range of Pocket Penetrometer (PPT) measurements performed in compacted BP-1 after each compaction experiment overlays with the range of the correlation testing. The values recorded for the 71 Hz tests lay beyond the useful range of the correlation plot.

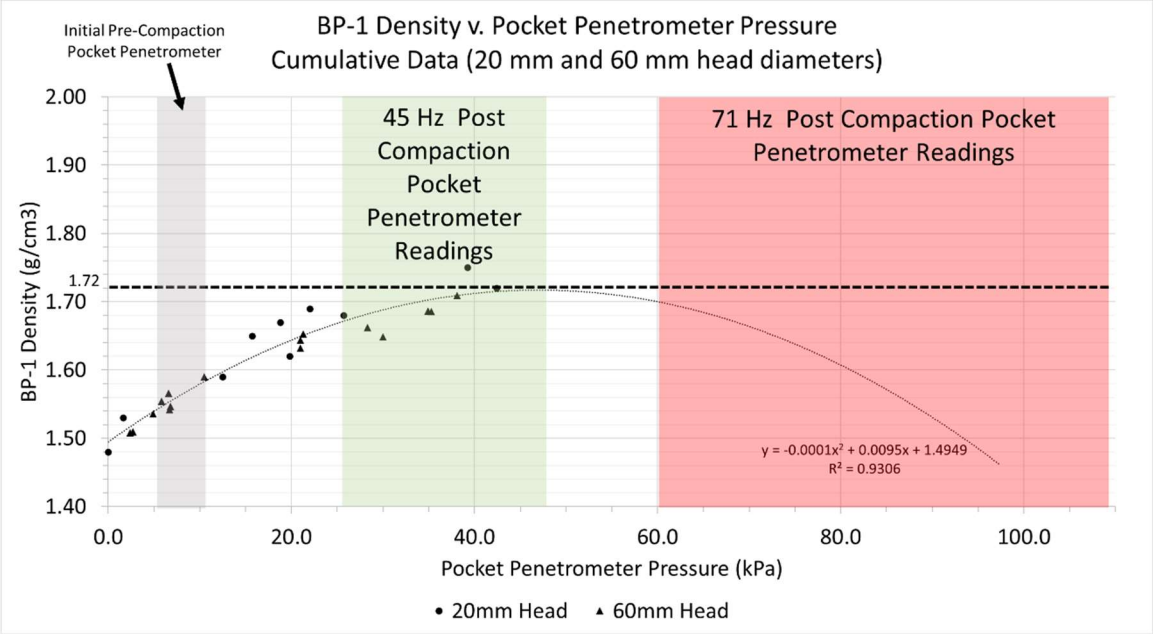

Figure 31. BP-1 density correlation and compaction data ranges for pocket penetrometer measurements.

The pocket penetrometer pressure values measured in BP-1 compacted at 71 Hz are significantly higher than the range exhibited for the values after 45 Hz compaction. The 45 Hz data is nearly all within the range of the correspondence curve generated and the quadratic equation fitting the data is valid within such range. However, the equation is no longer valid in the 71 Hz data range.

It is clear that complementary data must be collected for higher range pocket penetrometer values to complete the range of applicability of the correspondence plot for high bulk density BP-1 values. This requires modifying the compaction method which was not feasible within the timeframe of this phase of work.

The solution for extending the applicability range of the density-PPT relationship was found in the use of field core sampling data collected during the compaction tests that contained both PPT and gravimetric density measurements of regolith samples at the compacted sites. This data collection was performed with the 20-mm foot after 71-Hz compaction tests and covers the highest regolith densities recorded. These additional data were added to the correlation data set resulting in the extended range plot in Figure 32. The polynomial fit equation was adjusted to ensure that the density values corresponding to the highest PPT readings reflected the expected asymptotic behavior near the maximum density value of 1.86 g/cm3 recorded in our core sampling and in agreement with the value published by Suescun-Florez.

The resulting polynomial fit equation is as follows and was used in all PPT data analysis of compaction tests:

$$D = -4e^{-0}\ P_{pp}^2 + 0.0075P_{pp} + 1.5075$$

Where D is the surface bulk density of BP-1 and P_{pp} is the pressure reading from the pocket penetrometer.

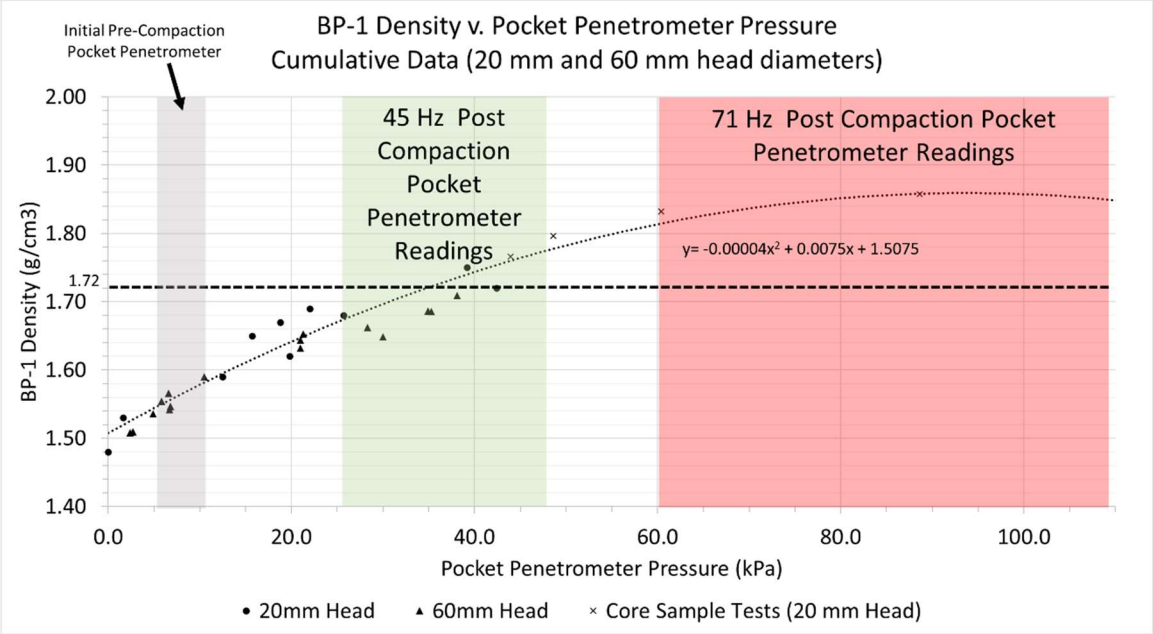

Figure 32. Compaction data ranges for pocket penetrometer measurements with core sample correlation included and custom trendline.

e. LHS-1 Density - Compression Strength Correlation

A limited version of the approach described above for BP-1 was taken to establish a density – compression strength curve for LHS-1. Core sample and 20 mm diameter head pocket penetrometer measurements that were made during testing in LHS-1. These measurements were used to establish the curve rather than an independent set of tests. These values are presented in Table 5 along with values that were taken from the BP-1 density- compression strength correlation curve (which are discussed below).

Table 5. LHS-1 pocket penetrometer correspondence data.

Test	Pressure (kPa)	Density (g/cm^3)	Note
C1	44.7	1.70	
C2	87.4	1.81	
C3	40.6	1.67	
C4	34.3	1.70	
C5	25.0	1.75	
C6	40.6	1.76	
BP-1 Data	0.001	1.48	Data taken during the BP-1 correspondence curve testing.

The resulting curve (excluding BP-1 Data) is presented in Figure 33. The curve is not characteristic of the actual pressure – density relationship in LHS-1 because no data points were available towards the low range of the x axis. A data point from the low-pressure region of the BP-1 density – pressure correspondence curve testing was added to correct the curve. The addition of this point is justified given the highly variable nature of geotechnical data collection

methods and the similar geotechnical properties between LHS-1 and BP-1 as described throughout the literature. The new curve is presented in Figure 34. It should be noted that the only place this curve was used in the analysis performed under this study was to provide an initial pre-compaction absolute density of LHS-1 (which was converted to relative density) to use in Figure 26 which allowed for a comparison of spot compaction performance in LHS-1 v. BP-1 at 71 Hz in ambient.

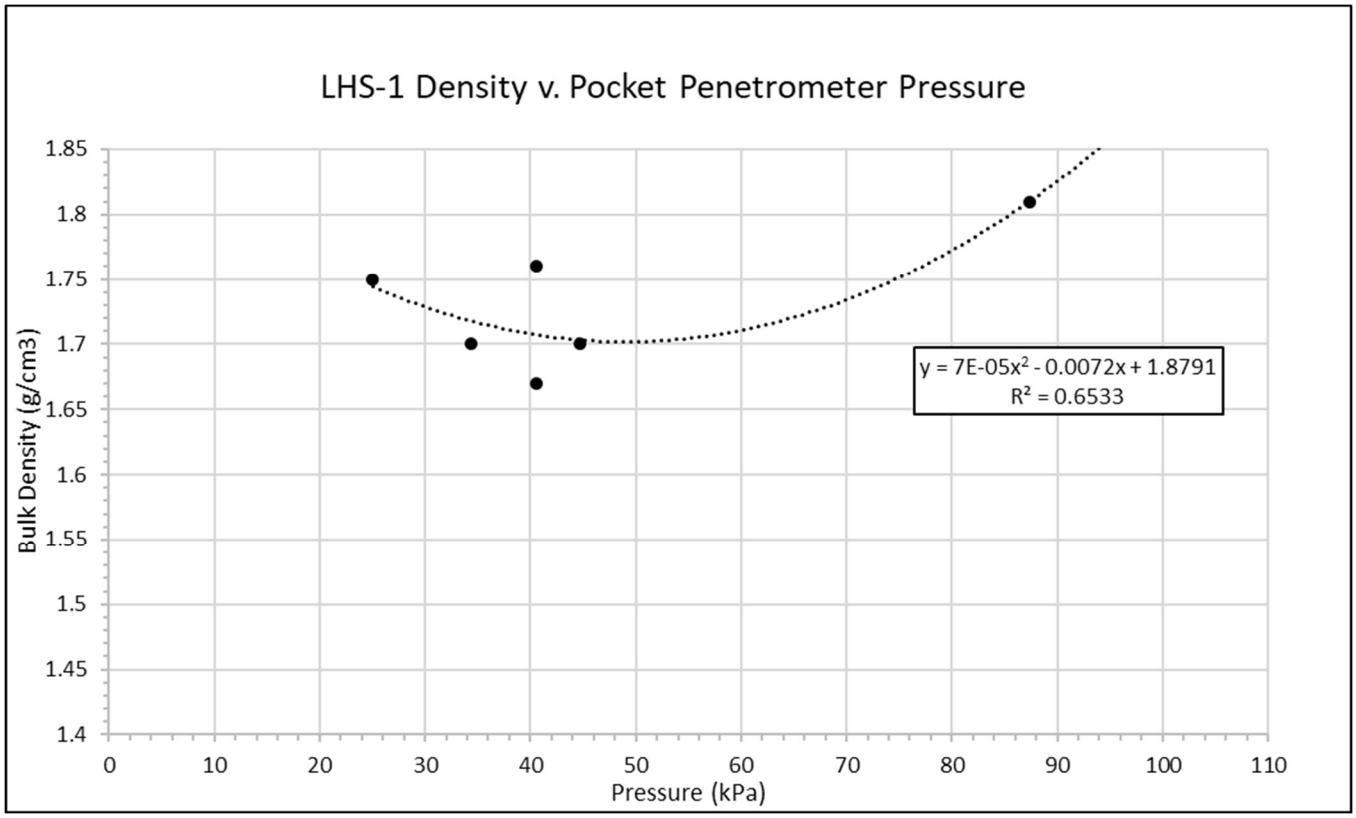

Figure 33. LHS-1 density v. pocket penetrometer pressure without BP-1 based y-intercept point.

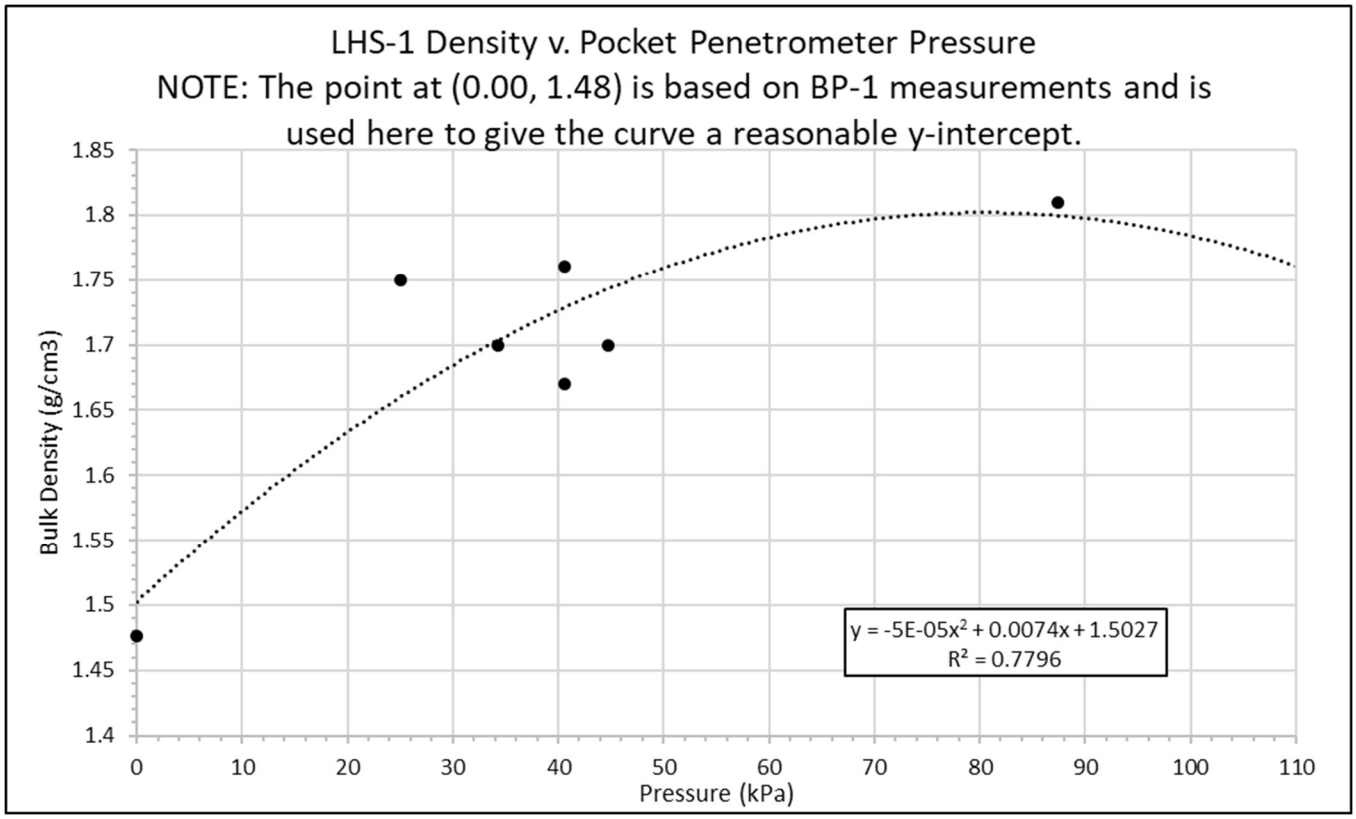

Figure 34. LHS-1 density v. pocket penetrometer pressure with BP-1 based y-intercept point.

10. Appendix B: Relative Density Calculations

Relative density was calculated using the following equation from ASTM D4254, 2016 [9]:

$$\rho_R = \left(\frac{\rho_{max}}{\rho} x \frac{\rho - \rho_{min}}{\rho_{max} - \rho_{min}}\right) x100\%$$

where ρ_R is the relative bulk density, ρ_{max} is the maximum bulk density, ρ_{min} is the minimum bulk density, and ρ is the measured bulk density.

a. BP-1 Relative Density

ρ_{min} for BP-1 was reported as 1.27 g/cm^3 using ASTM D4254 method A [8]. The same publication reported ρ_{max} as 1.86 g/cm^3 using the Kolbuszewski dry method [10]. Using these values 80% relative density correlates to an absolute density of 1.70 g/cm^3 for BP-1. A relative density of 48% correlates to an absolute density of 1.50 g/cm^3.

b. LHS-1 Relative Density

LHS-1 maximum and minimum densities were the same as BP-1 [11] with ρ_{min} for LHS-1 reported as 1.27 g/cm^3 using ASTM D4254 method C and ρ_{max} as 1.86 g/cm^3 using a mechanical tapping method. Using these values 80% relative density correlates to an absolute density of 1.70 g/cm^3 for LHS-1. A relative density of 48% correlates to an absolute density of 1.50 g/cm^3.